UC San Diego

UC San Diego Previously Published Works

Title

Ultrashort echo time magnetic resonance imaging of the osteochondral junction

Permalink

https://escholarship.org/uc/item/3c95916p

Journal

NMR in Biomedicine, 36(2)

ISSN

0952-3480

Authors

Lombardi, Alecio F

Guma, Monica

Chung, Christine B

et al.

Publication Date

2023-02-01

DOI

10.1002/nbm.4843

Peer reviewed

eScholarship.org Powered by the California Digital Library
University of California

Author Manuscript

Author Manuscript

Author Manuscript

Author Manuscript

HHS Public Access

Author manuscript

NMR Biomed. Author manuscript; available in PMC 2024 February 01.

Published in final edited form as:

NMR Biomed. 2023 February ; 36(2): e4843. doi:10.1002/nbm.4843.

Ultrashort Echo Time MR Imaging of Osteochondral Junction

Alecio F. Lombardi[1,2], **Monica Guma**[2,3], **Christine B. Chung**[1,2], **Eric Y. Chang**[1,2], **Jiang Du**[1], **Ya-Jun Ma**[1]

[1.] Department of Radiology, University of California San Diego, CA, United States

[2.] Research Service, Veterans Affairs San Diego Healthcare System, CA, United States

[3.] Department of Medicine, University of California San Diego, CA, United States

Abstract

Osteoarthritis is a common chronic degenerative disease that causes pain and disability with increasing incidence worldwide. The osteochondral junction is a dynamic region of the joint that is associated with the early development and progression of osteoarthritis. Despite the substantial advances achieved in the imaging of cartilage and application to osteoarthritis in recent years, the osteochondral junction has received limited attention. This is primarily related to technical limitations encountered with conventional MR sequences that are relatively insensitive to short T2 tissues and the rapid signal decay that characterizes these tissues. MR sequences with ultra-short echo time (UTE) are of great interest since they can provide images of high resolution and contrast in this region. Here we briefly review the anatomy and function of cartilage, focusing on the osteochondral junction. We also review basic concepts and recent applications of UTE MR sequences focusing on the osteochondral junction.

Keywords

UTE; MRI; osteochondral junction

1. Introduction

Osteoarthritis (OA) is a chronic degenerative disease that causes functional disability and pain, affecting approximately 300 million people worldwide[1]. The pathogenesis is not fully understood, and despite great investment in the development of therapeutic agents, to date, no effective treatment to slow progression is available[2].

Imaging characterization of osteoarthritis, on the other hand, has evolved significantly in the past ten years, moving from a strictly morphologic evaluation towards a more thorough analysis, including both morphologic and quantitative features of the joint[3]. These advances are attributed to technological developments in both hardware and software of MR systems. Today, high-resolution and quantitative MR sequences allow for the assessment of small structures with high image quality as well as for the measurement of relaxation times of

Corresponding author: Alecio F. Lombardi, MD, alecio.lombardi@icloud.com, University of California, San Diego, La Jolla, CA 92037, Phone: (858) 246-2229.

Author Manuscript Author Manuscript Author Manuscript Author Manuscript

cartilage and other joint tissues[4–6]. 3D dual-echo in steady-state (DESS) MR sequences, for example, permit the evaluation of cartilage morphology with high contrast and spatial resolution[5]. T2 and T1rho relaxation time measurements can estimate the relationship between water, collagen, and glycosaminoglycans/proteoglycans in cartilage[3,7]. These are only a few examples of many new techniques and tools currently available to radiologists, clinicians, and surgeons for better clinical diagnosis and treatment than before.

MRI is established now as the imaging modality of choice in the diagnosis of OA[8], but few studies focus on the evaluation of the osteochondral junction (OCJ), a thin layer of transition between cartilage and bone, essential in OA pathogenesis and progression[9]. It is across the osteochondral junction that the transport of nutrients from the subchondral bone to the avascular cartilage occurs, helping maintain its homeostasis and function. It is also at the OCJ where ossification of cartilage begins at the early stages of OA, later progressing towards the middle and superficial layers, contributing to the formation of central osteophytes and ultimately to cartilage and joint stiffness, characteristic of OA[10,11]. Dedicated imaging studies of the OCJ are few due to technical challenges related to the required resolution and contrast mechanisms needed to fully evaluate this region[12]. Recent studies, for example, showed a high variability of T2*, T1rho, and T1 measurements in deeper layers of cartilage when conventional spin-echo (SE) MR sequences were used because of the low signal-to-noise ratio (SNR) in these regions [13]. When ultra-short echo time (UTE) MR sequences were used, however, the errors of measurements were much reduced for these same deep regions of cartilage[13].

UTE MRI is of great interest in the evaluation of OCJ as UTEs allow the acquisition of signals of this region with higher SNRs. When dual-echo or inversion recovery (IR) pulses are used, higher contrast is achieved compared to SE sequences[14]. Moreover, UTE MRI offers great flexibility in choosing the echo time and includes different types of magnetization preparation modules, such as the magnetization transfer (MT) preparation to estimate the macromolecular fraction (MMF) of cartilage[15], making possible the quantitative evaluation of OCJ with a variety of imaging biomarkers.

This review aims to briefly revisit the OCJ anatomy and function, as well as its role in early OA development. We also summarize recent MRI developments for OCJ assessment both morphologically and quantitatively. We will also discuss the main advantages and limitations of UTE MRI, pointing towards future directions in research and clinical applications regarding OCJ imaging and the diagnosis and treatment of OA.

2. Cartilage Anatomy and Function

The cartilage is an avascular and aneural tissue consisting mostly of water, with variable thickness depending on the anatomical region and the mechanical stress to which it is subjected[16,17]. The cartilage thickness varies in different joints: knee, 1.69 to 2.55 mm[17]; ankle, 1.0 to 1.69 mm[17]; hip, 1.08 to 2.4 mm[18]; and shoulder, 1.0 to 1.9 mm[19,20]. In the knee, the mean cartilage thickness varies from 1.69 mm to 2.55 mm, whereas, in the ankle, its thickness ranges from 1.0 to 1.69 mm[17]. Collagen and proteoglycans combine to form a complex network that retains water and gives cartilage its viscoelastic properties. It can

Author Manuscript Author Manuscript Author Manuscript Author Manuscript

endure high shear and compressive forces, reducing the stress transferred to the joint and subchondral bone[21]. The loss of cartilage integrity, either by acute or chronic trauma or inflammation, will likely cause dysfunction of its load-deformation viscoelastic behavior and lead to osteoarthritis.

Normal cartilage is divided into four zones from the articular surface to the osteochondral junction: superficial, transitional, radial, and calcified[22] (Figure 1). The superficial zone comprises approximately 10% of the total cartilage thickness and presents a higher chondrocyte and water concentration but a lower proteoglycan content. The superficial layer is in contact with the intra-articular space and protects deeper layers from trauma and loss of tissue integrity. The transitional zone thickness varies according to different studies and authors in the literature, with some pointing to 10–20% of the total cartilage thickness and others indicating 30–50% of the cartilage thickness[22]. This zone presents higher proteoglycan concentration and thicker collagen fibers which are obliquely oriented compared to the superficial zone (Figure 1). The transitional zone offers resistance to compressive forces[23]. The radial zone thickness varies according to different reports, ranging from 30–40% to 80% of the total cartilage thickness[22,23]. In this zone, the proteoglycan concentration is the highest of all zones, and the collagen fibers are the thickest, oriented perpendicular/radially to the articular surface[22,24–26] (Figure 1). The water concentrations are lower than in the other two zones, but the radial zone has the strongest resistance to mechanical stress due to a complexly interlinked lattice of collagen fibers and proteoglycans[25]. There are also some variations in laminar composition or zone ratios between femoral and tibial cartilage[26].

The structures of uncalcified cartilage, zone of calcified cartilage (ZCC), and bone region are well displayed in high-resolution scanning electron microscopy (SEM) images[27], as can be seen in Figure 2. The calcified zone is highly mineralized, consisting of 5–8% of the total cartilage thickness. A wavy line limiting the end of the uncalcified radial zone and the beginning of the calcified zone is commonly referred to as the “tidemark”. On the other side, the calcified zone is attached to the underlying bone through interdigitations that invaginate into the subchondral bone, also called the “cement line”. The main functions of the calcified zone are to transfer mechanical stress across the bone-cartilage interface[28,29] and transport nutrients through vascular channels that permeate this region, from subchondral bone to cartilage[30]. In OA, the calcified zone proliferates and advances towards the radial zone[31] creating the so-called “duplicated tidemark”. Also, in OA, the vascular channels that normally exist only in the calcified zone can increase in number and length, advancing into the radial zone of cartilage[11,29]. Those processes contribute to an increase in joint stiffness and transport of inflammatory agents, respectively, two hallmarks of OA. Studies also suggest that ossification and spicules (i.e., the aggregates of the bony matrix, seen in Figure 2B) originating from the calcified zone protrude into the radial layer, causing microtrauma that may initiate or accelerate cartilage degeneration and can also contribute to bone remodeling, new bone formation, and the origin of central osteophytes[10,11] (Figure 3). The hypothesis of bone remodeling and new bone formation in OA is corroborated by findings that those spicules are commonly accompanied by vascular channels, resembling the process of primary bone formation in fracture healing[31]. Strong evidence suggests that subchondral bone cysts and bone marrow edema are closely related to OA and

Author Manuscript Author Manuscript Author Manuscript Author Manuscript

bone remodeling, highlighting the important role the zone of calcified cartilage and the subchondral bone plate have in the pathogenesis of OA[32].

The chondrocytes are responsible for the production of the extracellular matrix (collagen and proteoglycans) that helps retain water. Water, on the other hand, is essential to sustain mechanical loading as its interaction with collagen and proteoglycan increases the cartilage viscoelasticity[33], allowing greater stress resistance. Water is cartilage's most abundant component varying from 80% of its weight in the superficial zone to about 65% of its weight in the radial zone[21,34]. When the integrity of the superficial zone of cartilage is compromised, a decrease in water content may occur and accelerate the degeneration process.

The OCJ is a fluid term referring to the transition between the deep layers of cartilage and bone, which includes the deep layers of the radial zone, the tidemark zone, the calcified cartilage, the cement line, and the subchondral bone plate[35,36]. Considering the important structures contained in this region and their relationship to the initiation and progression of OA, imaging methods focusing on the OCJ are of great interest. However, its small dimensions, the low water concentration, and the high mineralization of the calcified zone and the subchondral bone plate lead to volume average artifacts and low SNR on conventional MR sequences, commonly used to assess cartilage morphology and relaxometry, such as T2-weighted, PD-weighted, or T2 and T1rho mapping. Potential solutions to this problem include the use of high-resolution MR sequences with UTEs that can capture the rapid decaying signals from the structures of the OCJ.

4. UTE Imaging of the Osteochondral Junction

Conventional fast spin echo (FSE) MRI sequences such as T2-weighted or PD-weighted sequences can detect signals from tissues with T2 values as low as 8–10 ms, so tissues with shorter T2s appear of low signal intensity on those sequences[37,38] (Figure 4A and 4B). Gradient echo sequences can reduce the TE by an additional 1–2 ms, which is still not efficient for imaging water within the collagen fibers in the deep layers of the radial zone and the calcified zone of cartilage (T2 values of less than 1 ms)[38]. It is important to note that even the superficial cartilage with its higher free water content will include small amounts of water bound to collagen matrix that have short T2s, which are not detectable with conventional MR sequences. UTE sequences, on the other hand, can detect signals from these regions with high efficiency because it deploys TEs much lower than 1 ms, reaching values of 8 μs[39] (Figure 4C). Zero echo-time (ZTE) is another type of UTE sequence that can acquire signals from these tissues with short T2 values. Through the application of gradients before the radiofrequency pulse, the ZTE sequence has an echo time of near zero because the image acquisition begins with the gradients already ramped up[40,41]. A diagram showing 2D UTE, 3D UTE, and ZTE MRI sequences is presented in Figure 5. These new sequences have now been applied to routine clinical scenarios for validation[42]. Although there are technical requirements for implementation, the fast development and cost reduction of MR hardware and software will increase their availability in the future.

Author Manuscript Author Manuscript Author Manuscript Author Manuscript

Bae et al. have systematically reviewed pre-2014 UTE techniques for OCJ imaging in both knee and spine joints[43]. Most of these studies were conducted on ex vivo samples. Recently, many investigators have performed translational studies focused on morphological and quantitative imaging of the OCJ. In this review, we largely focused on the review of knee OCJ studies, especially for the most recent 3D UTE imaging developments.

3.1 Morphological UTE MRI

The first studies to use UTE MR sequences to evaluate human cartilage were from Brossman et al.[44] and Gold et al.[45]. Brossman et al. used a short echo time (TE of 150 μs) with k-space projection reconstruction for image acquisition of short T2 tissues in 7 min and 30 sec and compared it with a fat-suppressed gradient recalled echo in the steady-state (Spoiled GRASS) sequence for detection of cartilage lesions, using histopathologic grading as reference. They found greater sensitivity, specificity, and accuracy of the short echo time sequence compared to Spoiled GRASS ($p = 0.03$) for the detection of cartilage lesions with a perfect inter-reader agreement. The investigators hypothesized that short echo time with projection reconstruction could detect earlier disruption of collagen structures because of the detection of water linked to collagen associated with very short T2 values[44]. Gold et al., on the other hand, used a 3D UTE cones sequence with a non-cartesian k-space sampling, a TE of 0.6 ms that took 9.7 min of scan time for image acquisition[45]. They found that the 3D cones sequence was suited to scan the whole knee cartilage with high resolution and isotropic multiplanar reconstruction showing cartilage damage as well as abnormalities in the deep layers and OCJ.

The first implementation of 2D UTE MRI sequences used two half-pulse radiofrequency (RF) excitations with gradients in opposite directions, followed by a radially acquired projection reconstruction to produce images with very short TEs[46–48] (Figure 5A). Additional methods to suppress the long T2 components of tissues were proposed. The first was a long rectangular 90° RF pulse followed by gradients to dephase the long T2 magnetizations and emphasize signals from short T2 components. The second was a long initial inversion pulse to selectively null the long T2 magnetization (“magnetization preparation”), followed by image acquisition when this long T2 magnetization crossed the null point, highlighting only short T2 magnetization. The third was the acquisition of images in two subsequent echo times, followed by subtraction between signals of the two echoes (“dual-echo”), leaving only the signals from short T2 species[48].

Fat is highly concentrated in the subchondral bone marrow and other periarticular joint tissues. In non-Cartesian UTE sequences, chemical shift artifacts can “move” the strong fat signal towards the OCJ. This can deteriorate the image quality and introduce errors in relaxometry measurements of the OCJ. Fat suppression is thus critical on UTE MRI and can be obtained through various methods, including but not limited to fat saturation[49], water excitation[50,51], the Dixon method[52], or inversion recovery pulses[53].

Gatehouse et al. studied the fat-suppressed 2D UTE MRI with radial center-out k-space sampling. Dual-echo subtracted knee MR images were obtained from five volunteers and 16 patients in a scan time of 8.5–17 min. They found that the cartilage on subtracted images showed two distinct layers: superficial with intermediate signal intensity and deep with high

Author Manuscript Author Manuscript Author Manuscript Author Manuscript

signal intensity. This high signal intensity layer had variable thickness, greater in the tibial plateau. Cartilage lesions were observed in both layers with high conspicuity, including cartilage defects and hemorrhage in the deep layers on UTE MRI[54].

Rahmer et al. compared the efficiency between “dual-echo” and “magnetization prepared” approaches of 2D UTE MRI to improve short T2 contrast at 1.5 and 3.0 T. The “dual-echo” sequence used echo times of 50μs/4.6 ms and 50μs/2.3 ms, at 1.5 and 3.0 T, respectively, in a scan time of 8 min. The “dual-echo” method had a lower scan time (higher scan efficiency) than the “magnetization prepared” method. This is because the “magnetization prepared” sequence needs a long T1 recovery time between the magnetization preparation pulses to improve SNR[55]. Although some investigators report higher SNR on “magnetization prepared” sequences, the authors did not confirm this finding in their study, where both “dual-echo” and “magnetization prepared” sequences had similar SNR. However, “magnetization prepared” sequences showed a failure of long-T2 suppression close to the edges of the FOV, especially for larger FOVs at higher field strengths, possibly caused by off-resonance effects that are large enough to shift the long-T2 water frequency components outside the narrow band of the long-T2 suppression pulses[55].

Larson et al. developed a method of long T2 suppression using an adiabatic inversion preparation pulse that is insensitive to B1 inhomogeneities[56]. The adiabatic pulse is characterized by frequency and amplitude modulation that keeps the magnetization aligned or perpendicular to the effective radiofrequency pulse[56]. Longer T2 tissues will be more affected by the inversion pulse, while short T2 tissues will only present some signal attenuation, highlighting short T2 components. They used a TE of 50 μs in a scan time of 5 min and 20 sec. Despite being insensitive to B1 inhomogeneities, the adiabatic inversion pulse produces images with similar SNR and presents similar sensitivity to off-resonance effects compared to images generated with non-adiabatic inversion pulses.

Du et al. later described a method of long T2 suppression using two adiabatic inversion pulses, centered on the frequency of water and fat, respectively, using a 2D UTE MR acquisition at 3T, called dual inversion recovery ultrashort echo time (DIR-UTE) MRI[53]. With experimentally determined inversion times (TI) for the two IR preparations, the long T2 water and fat magnetizations reach a null point simultaneously. The total scan time was 5 min. They showed that the DIR-UTE MR sequence suppressed long-T2 water and fat tissues simultaneously with high efficiency, highlighting the deep layers of the radial zone of cartilage and the calcified zone with higher contrast compared to sequences using only one inversion recovery pulse[53].

One particular characteristic of cartilage imaging using UTE MRI is that the OCJ region demonstrates a high signal intensity linear appearance. This bright line becomes progressively more conspicuous and with greater contrast in relation to the superficial layers of cartilage on “dual-echo” UTE MRI[38], T1-weighted UTE MRI[57], single inversion recovery (IR) UTE MRI[58], and dual inversion recovery (DIR) UTE[59] (Figure 6). The explanation for the increase in the contrast performance across those UTE sequences includes the superiority of inversion pulses in the suppression of long T2 components of tissues compared to echo subtraction or frequency selective fat saturation.

Author Manuscript Author Manuscript Author Manuscript Author Manuscript

The first study to investigate the tissues giving origin to the high signal intensity detected in the deep layers of cartilage on UTE MRI was performed by Bae et al.[14]. The investigators assessed cadaveric patellae containing calcified cartilage and compared them to harvested cadaveric patellae containing uncalcified cartilage only, calcified cartilage plus subchondral bone, uncalcified cartilage plus calcified cartilage plus subchondral bone, and bone only. Histologic sections of the tissues were used as a reference. In the prepared samples, only bone-only samples did not exhibit high signal intensity on UTE images, suggesting that the bright line originated from the deep layers of the radial zone and the calcified zone of cartilage[14] (Figure 7). The confirmation of the origin of the bright line on UTE MRI has implications in determining a cut-off point separating normal and abnormal OCJ thickness in normal and osteoarthritic patients, as well as in the assessment of successful or unsuccessful cartilage repair surgery. However, the interpretation of findings on UTE MRI of the OCJ must be conducted carefully when no fat suppression is applied since chemical shift artifacts originating in the subchondral bone marrow, as mentioned before, can contaminate signal in the OCJ (Figure 8).

A conspicuous image of the OCJ is highly desirable as this region may have a thickness of less than 0.5 mm in some anatomical regions. In this regard, 3D sequences have a few potential advantages over 2D sequences: first, the slices are contiguous without gap, reducing the volume averaging; second, the SNR is higher than in 2D sequences, which increases the in-plane resolution; third, the isotropic acquisition of 3D sequences allows multiplanar reconstruction, which increases the conspicuity of small cartilage lesions[5]. A systematic review and meta-analysis comparing the performance of 3D and 2D conventional FSE MRI using arthroscopy and/or open surgery as the standard of reference showed higher sensitivity and specificity of 3D multiplanar reformatted images compared to 2D MR sequences ($p < 0.05$)[60]. The association between 3D and UTE MRI can add the same advantages obtained on 3D FSE MRI, including less volume averaging, higher SNR, and multiplanar reconstruction[61].

MacKay et al. studied the deep cartilage of the knee using 3D UTE MRI in 10 patients with knee pain and 10 healthy controls[62]. The investigators showed that healthy controls had a bright line on the deep cartilage more frequently and with higher signal intensity than patients with knee pain ($p = 0.001$ and $p < 0.001$, respectively). They also performed T2 mapping of the whole cartilage, not the OCJ, individually and compared both groups. The group with knee pain had higher mean T2 values in the medial tibial plateau than the asymptomatic group ($p < 0.001$).

Recently, Cai et al. developed a 3D T1-weighted fat-saturated (FS) UTE cones MR sequence capable of resolving the OCJ in a fast scan time (3 min), with high resolution and contrast[57]. In this study, the investigators found that incremental increases in the flip angle from 5 to 30 degrees resulted in higher signal intensity within the bright line representing the OCJ (Figure 9). This increment was higher for the OCJ than for other cartilage layers. The contrast-to-noise ratio (CNR) of the OCJ was high in healthy volunteers and low in OA patients (18.1 ± 3.5 between the OCJ and superficial cartilage and 26.7 ± 4.3 between OCJ and subchondral bone). They also performed T1 relaxometry of the cartilage and found a T1 value of 514 ± 7 ms in the OCJ, compared to 890 ms ± 15 in the superficial layer of

Author Manuscript Author Manuscript Author Manuscript Author Manuscript

cartilage. A great advantage of this sequence is its time efficiency derived from the use of shorter TRs typical of T1-weighted sequences, with a scan time of only 3 min.

Ma et al. developed a 3D T1-weighted adiabatic inversion recovery prepared fat-suppressed UTE Cones sequence (3D IR-FS-UTE) for high resolution and contrast imaging of the OCJ [58]. The inversion pulse was centered on the frequency of water to suppress signals from the long T2 tissues mostly from the superficial cartilage, and to highlight the osteochondral junction (Figure 10). A fat saturation module was also used to suppress signals from the subchondral bone marrow fat. The scan time was 9 min 8 sec. The authors also performed T1 relaxometry of the OCJ and found a value of 405 ± 16 ms. The IR-FS-UTE image showed a higher contrast between OCJ and superficial cartilage (20.1 ± 7.4) than the 3D T1-w FS UTE Cones sequence (18.1 ± 3.5) but a similar contrast between the OCJ and the subchondral bone (25 ± 9.6 versus 26.7 ± 4.3 of the T1-w FS UTE Cones). The higher contrast came with a compromise in the scan time efficiency (9 min 8 sec versus 3 min of the T1-w FS UTE Cones) due to the higher TRs necessary for the recovery of the inversion pulses[58].

Lombardi et al. implemented a 3D DIR-UTE Cones sequence in which a second inversion pulse centered on the frequency of fat was used in addition to the pulse centered on the water frequency to increase further the contrast of the osteochondral junction[59] (Figure 11). Here the second IR pulse replaced the fat saturation module from the IR-UTE, increasing the efficiency of suppression of signals from the subchondral bone marrow fat. The total scan time was 9 min and 58 sec. The 3D DIR-UTE cones sequence showed a significantly higher CNR between the OCJ and the subchondral bone (mean, SD: 25.7 ± 2.3) and between the OCJ and superficial cartilage (mean, SD: 22.2 ± 3.5) compared with the 3D IR-FS-UTE sequence (mean, SD: 10.8 ± 2.5 and 16.3 ± 2.6, respectively). The higher CNR made the interruption of the bright line representing the OCJ more evident in patients with osteoarthritis (Figure 12).

UTE MRI has also been used in animal models after intra-articular injection of superparamagnetic iron oxide nanoparticles (SPIOs) for the evaluation of treatment of osteochondral defects using iron-labeled mesenchymal stem cells[63]. The rapid signal decay from the iron oxide nanoparticles makes them difficult to detect on conventional MR sequences but perfect for analysis using UTE sequences. According to preliminary results, UTE MRI was able to detect the OCJ and the associated iron-labeled stem cells with excellent anatomical detail.

A summary of all the above morphological UTE imaging studies can be seen in Table 1.

The morphological UTE imaging methods, including the subtraction, T1 weighting, and IR-based techniques, are able to highlight the OCJ regions with high resolution. Signal or structural changes in the OCJ region have been detected for abnormal cartilage using these techniques. Future clinical validation studies with a large cohort would provide more information about the potential value of these UTE OCJ imaging techniques.

Author Manuscript Author Manuscript Author Manuscript Author Manuscript

3.2 Quantitative UTE MRI

Compositional imaging of cartilage using UTE MRI has also been studied. Du et al. investigated 2D DIR UTE MRI for the assessment of T1, T2*, and T1rho mapping in the zone of calcified cartilage in cadaveric patellae[39]. The investigators found that the zone of calcified cartilage had a short T2* ranging from 1.0 to 3.3 ms, a short T1 ranging from 256 to 389 ms, and a short T1rho ranging from 2.2 to 4.6 ms, providing a non-invasive indirect assessment of water content and collagen orientation (through T2* measurements) as well as the proteoglycan content estimation (may use T1rho as a biomarker) of this region (Figure 13).

In a study with 42 participants (31 patients undergoing anatomic anterior cruciate ligament reconstruction (ACLR) and 11 uninjured controls), the cartilage of the medial femoral condyle and the medial tibial plateau was evaluated with 3D UTE-T2* mapping using arthroscopic data as reference[64]. The arthroscopic Outerbridge classification of cartilage degeneration was used: grade 0 = normal, grade 1 = cartilage softening and swelling, grade 2 = partial thickness defect with fissures on the surface that do not reach subchondral bone or exceed 1.5 mm in diameter, grade 3 = fissuring to the subchondral bone in an area with a diameter greater than 1.5 mm, and grade 4 = exposed subchondral bone. The cartilages of the central and posterior medial femoral condyle (cMFC and pMFC, respectively), as well as the central and posterior medial tibial plateau (cMTP and pMTP, respectively), were segmented into superficial and deep layers. The mean deep and superficial UTE-T2* values did not vary significantly with the cartilage injury status and arthroscopic grade among ACL-reconstructed patients ($p > 0.05$). However, among the participants with intact cartilage, UTE-T2* values discriminated between uninjured controls, patients with Outerbridge grade 0, and ACL-injured patients with Outerbridge grade 1 ($p = 0.01$). UTE-T2* values in the deep cartilage of the cMFC of ACL-injured patients with Outerbridge grade 0 were higher than in uninjured controls (15.3 ms ± 4.8 vs. 9.9 ms ± 2.3, respectively; $p = 0.01$). UTE-T2* values in the deep cartilage of the pMFC of ACL-injured patients with Outerbridge 1 were significantly higher than in uninjured controls (19.9 ms ± 7.7 vs. 11.9 ms ± 2.4, respectively; $p = 0.01$). Moreover, the UTE-T2* values in deep pMFC cartilage of injured patients decreased to levels similar to those in uninjured controls on longitudinal post-operative assessment ($p = 0.02$), suggesting healing[64].

3D UTE-T2* values in the deep cartilage of the knee seem not only to be elevated in degenerated cartilage but also to be associated with knee mechanical alignment and knee adduction moment (KAM) during walking, two well-known clinical markers of increased risk of knee OA, in patients subjected to ACLR[65] (Figure 14). Specifically, higher varus knee alignment is associated with a higher risk of OA[66], whereas a higher peak of KAM in OA patients is associated with faster progression and greater severity of OA[67,68]. The results of this study showed that UTE-T2* values in ACL-reconstructed knees were elevated in the cMFC and pMFC compared with uninjured knees ($p = 0.003$ and $p = 0.012$, respectively). UTE-T2* values in the cMFC cartilage of ACL-reconstructed patients positively correlated with increasing varus alignment ($R = 0.568$). Moreover, greater UTE-T2* values in the cartilage of ACL-reconstructed patients also correlated with higher KAM first and second peaks during walking ($R = 0.452/0.465$ and $R = 0.463/0.764$ for cMFC and cMTP,

Author Manuscript Author Manuscript Author Manuscript Author Manuscript

respectively). Another study of UTE-T2* values in the deep cartilage in the patellofemoral joint showed a significant correlation with worse Knee Injury and Osteoarthritis Outcome Scores for Sports/Recreation (KOOS sport/rec) n (rho = - 0.32, p = 0.015), and with gait metrics, again in patients submitted to ACLR[69]. The authors concluded that patellofemoral deep cartilage matrix disruption, assessed through UTE-T2*, was associated with reduced sports and recreational function and altered gait metrics.

Badar et al. investigated the magic angle effect in T2* measurements of UTE in the region of transition between cartilage and subchondral bone using μMRI and polarized microscopy. They compared the results of UTE with those of gradient recalled echo (GRE) and FSE MRI[12]. The investigators found that UTE was the only sequence capable of reliably measuring T2* of the deep radial and calcified zones of cartilage. When the B_0 was oriented at 55° in relation to the cartilage sample, however, the T2* values were slightly higher at the zone of the tidemark, possibly due to magic angle effects. Nevertheless, the magic angle phenomenon seems to have little effect on UTE MRI sequences, especially using bi-exponential methods for model fitting. Shao et al. studied the effect of the magic angle in T2* measurements of cartilage using bi-exponential fitting and found that the long T2* values tended to increase from subchondral bone to the superficial cartilage, but short T2* remained stable[70] (Figure 15). Also, they found that long T2*s and T2s showed a significant magic angle effect for all layers of cartilage, while short T2* values were insensitive to the magic angle effect.

More recently, Lombardi et al. studied T1, T1rho, MMF, and T2* of the OCJ in 35 human cadaveric knees using 3D UTE MRI[71]. The authors showed that T1, T1rho, and T2* relaxation times as well as the MMF of OCJ regions, were significantly different from those of the superficial cartilage ($p < 0.001$). T1, T1rho, and T2* relaxation times increased from deep to superficial cartilage, while MMF decreased from the OCJ to superficial cartilage. Moreover, there was a significant positive correlation between T1, T1rho, and T2* relaxation times and the cartilage degeneration MRI Osteoarthritis Knee Score (MOAKS), whereas the MMF showed a significant negative correlation[71].

A summary of all the above quantitative UTE imaging studies can be seen in Table 2.

These results show that UTE is able to measure compositional features of deep layers of cartilage and that those measurements may reflect relevant clinical characteristics in osteoarthritic patients. Thus, UTE MRI can complement conventional MRI in the quantitative assessment of early cartilage degeneration. Although most of the current research on UTE focused on T2* measurements of the OCJ, which reflects the water composition and collagen orientation of cartilage, the consistent results encourage the expansion of studies to other important biomarkers such as T1rho, MMF, and glycosaminoglycan chemical exchange saturation transfer (gagCEST) that reflect the proteoglycan, collagen, and glycosaminoglycan content, respectively.

When studying the transition between cartilage and bone with morphological or quantitative UTE sequences, there are variations among authors regarding constituents of the deep layers of the radial zone and the calcified zone[12,14,72,73]. This is understandable due to the small

Author Manuscript Author Manuscript Author Manuscript Author Manuscript

dimensions of these structures and the current limitations of spatial resolution of clinical MRI. Further developments in MRI hardware, especially RF coils and gradient systems, may provide definitive information.

4. ZTE Imaging of the Osteochondral Junction

3D ZTE MRI has also been used to image the OCJ. Similar to the IR-FS-UTE technique, Jang et al. implemented an adiabatic inversion recovery prepared ZTE MRI with fat saturation (IR-FS-ZTE) to highlight the OCJ region with high resolution and contrast, showing that the IR-FS-ZTE was superior to regular ZTE regarding the image contrast of this region[74]. ZTE image acquisition starts with the gradients already ramped up, so the TE is near zero. There are small increments of gradients between each repetition time and before each RF pulse, thus resulting in low acoustic noise (Figure 5C).

5. SWIFT Imaging of the Osteochondral Junction

Rautiainen et al. studied chondral and osteochondral defect healing in the intercarpal joints of horses for 12 months using 3D Sweep Imaging with Fourier Transform (SWIFT) at 9.4T[75]. This MRI sequence applies radiofrequency pulses with amplitude and frequency modulation, thus the name “Sweep”, associated with gradient increments, that allows the use of very short TEs with low acoustic noise, similar to ZTE MRI[76]. The SNR in the subchondral plate with SWIFT (0.91) was more than four times higher than with conventional FSE (0.12) and GRE (0.19) MR images[76]. The same group carefully co-registered the SWIFT MRI, μCT, and histology images for the OCJ samples[77]. They found that the bright SWIFT MRI signal at the OCJ region is not located in the calcified cartilage but on the deep layers of the radial zone in cartilage. The short T1 relaxation times of deep cartilage and susceptibility-induced effects arising from the calcified tissues could be the sources of this bright signal line. This study demonstrates that the signals in the bright line may originate largely from the deep layer cartilage. The calcified layer and subchondral bone may also make contributions to the bright signals due to the partial volume effect induced by the short T2 blurring and susceptibility-induced signal shifts in non-Cartesian imaging. These findings are in line with the most recent 3D UTE imaging studies [57–59].

5. Future of OCJ imaging

One of the potential applications of MR imaging of the OCJ is to evaluate the treatment for osteochondral defects, a common type of injury, especially in young patients, that evolves into osteoarthritis if not promptly treated. There are several treatment options available, including marrow stimulation, osteochondral autograft, osteochondral allograft, and autologous chondrocyte implantation, each with its specific indications[78]. To this date, the clinical evaluation of the treatment success is performed using morphological features on conventional FSE or GRE MR sequences and computed tomography[78]. Some studies have shown the potential of quantitative MRI techniques in the characterization of cartilage, a critical factor for treatment monitoring and clinical outcome prediction[79–81]. Combining these quantitative MRI techniques with UTE acquisition further allows the assessment of biochemical component (e.g., water, collagen, and proteoglycan) changes in the OCJ,

Author Manuscript Author Manuscript Author Manuscript Author Manuscript

providing information essential to clinical decision-making. Those quantitative sequences include T1rho, T2, T2* mapping, sodium imaging, delayed gadolinium-enhanced MRI of cartilage (dGEMRIC), gagCEST, and MT[15, 79–81]. Specialists' consensus on how to acquire, analyze, and interpret images of T1rho and T2 mapping focusing on the whole cartilage has already been published[7]. A few studies tried to correlate UTE-T2* of the deep cartilage with clinical outcomes. For example, UTE-T2* has been associated with knee mechanical alignment as well as KAM during walking[65,66], suggesting that it could be used to discriminate between uninjured controls and ACL-injured patients. Future research may combine UTE with other quantitative MR sequences (such as diffusion MRI[82]), focusing on the OCJ region only, bringing new insights into early abnormalities in the development of osteoarthritis and the assessment of treatment response.

Potential technical limitations of current UTE sequences are the need for high gradient and RF system performance[83]. The gradients must have high slew rates and amplitudes; otherwise, images may be subjected to long readouts induced short T2 blurring. Also, RF coils must switch between receive and transmit states (ring-down or recovery time) fast to allow for imaging with ultra-short TEs. Another potential technical limitation is the long scan time when inversion recovery pulses are used due to the long T1 of some species. However, the use of multiple k-space spokes after each inversion pulse has been described and can reduce this scan time[84].

6. Summary

MRI of the OCJ is challenging due to the short T2 of the tissue components in this region and its small dimensions, which requires dedicated sequences to address resolution and contrast issues. 3D UTE sequences can reduce volume averaging artifacts, improve SNR, and allow multiplanar reconstruction compared to 2D UTE. Recently, many 3D UTE sequences have been developed to image the OCJ morphologically with high resolution and contrast. More interestingly, a series of 3D quantitative UTE measurements, including UTE-T2*, UTE-T1, UTE-T1rho, and UTE-MT, has been developed to correlate compositional features (e.g., water, collagen, and proteoglycan) in the OCJ with clinical and surgical outcomes. These UTE biomarkers have great potential for early diagnosis of OA. In the future, the combination of multiple methods and further development of new MR hardware and software will allow discoveries and insights about this highly metabolically active yet little-studied joint region.

Acknowledgment

The authors acknowledge grant support from NIH (P30AR073761, R01AR062581, R01AR068987, R01AR075825, R01AR079484, and R21AR075851), the VA Clinical Science Research & Development Service (I01CX001388, I01RX002604, I01CX000625, and I01CX002211), and GE Healthcare.

Abbreviations:

UTE	Ultra-short Echo Time
OA	Osteoarthritis

Author Manuscript Author Manuscript Author Manuscript Author Manuscript

OCJ	Osteochondral Junction
DESS	Dual-echo in Steady-State
SNR	Signal-to-noise Ratio
SE	Spin-Echo
FSE	Fast Spin Echo
GRE	Gradient Recalled Echo
MT	Magnetization Transfer
MMF	Macromolecular fraction
IR	Inversion Recovery
DIR	Dual Inversion Recovery
GRASS	Gradient Recalled Echo in the Steady-State
FS	Fat Saturation
SPIO	Superparamagnetic Iron Oxide Nanoparticles
ACLR	Anterior Cruciate Ligament Reconstruction
KAM	Knee Adduction Moment
ZTE	Zero Echo Time
SWIFT	Sweep Imaging with Fourier Transform
dGEMRIC	Delayed gadolinium-enhanced MRI of cartilage
gagCEST	glycosaminoglycan Chemical Exchange Saturation Transfer
KOOS	Knee Osteoarthritis Outcome Score
MOAKS	MRI Osteoarthritis Knee Score

References

1. James SL, Abate D, Abate KH, et al. Global, regional, and national incidence, prevalence, and years lived with disability for 354 diseases and injuries for 195 countries and territories, 1990–2017: a systematic analysis for the Global Burden of Disease Study 2017. The Lancet. 2018;392(10159):1789–1858.
2. Jiang Y Osteoarthritis year in review 2021: biology. Osteoarthritis and Cartilage. 2021.
3. Roemer FW, Demehri S, Omoumi P, et al. State of the Art: Imaging of Osteoarthritis-Revisited 2020. Radiology. 2020;296(1):5–21. [PubMed: 32427556]
4. Gao KT, Pedoia V, Young KA, et al. Multiparametric MRI characterization of knee articular cartilage and subchondral bone shape in collegiate basketball players. J Orthop Res. 2021;39(7):1512–1522. [PubMed: 32910520]
5. Kijowski R 3D MRI of Articular Cartilage. Semin Musculoskelet Radiol. 2021;25(3):397–408. [PubMed: 34547805]

Author Manuscript Author Manuscript Author Manuscript Author Manuscript

6. Verschueren J, Van Langeveld SJ, Dragoo JL, et al. T2 relaxation times of knee cartilage in 109 patients with knee pain and its association with disease characteristics. Acta Orthop. 2021;92(3):335–340. [PubMed: 33538221]
7. Chalian M, Li X, Guermazi A, et al. The QIBA Profile for MRI-based Compositional Imaging of Knee Cartilage. Radiology. 2021;301(2):423–432. [PubMed: 34491127]
8. Oei EHG, Hirvasniemi J, van Zadelhoff TA, van der Heijden RA. Osteoarthritis year in review 2021: imaging. Osteoarthritis and Cartilage. 2022;30(2):226–236. [PubMed: 34838670]
9. Suri S, Walsh DA. Osteochondral alterations in osteoarthritis. Bone. 2012;51(2):204–211. [PubMed: 22023932]
10. Boyde A The Bone Cartilage Interface and Osteoarthritis. Calcif Tissue Int. 2021;109(3):303–328. [PubMed: 34086084]
11. Lombardi AF, Tang Q, Wong JH, et al. High-Density Mineralized Protrusions and Central Osteophytes: Associated Osteochondral Junction Abnormalities in Osteoarthritis. Diagnostics. 2020;10(12):1051. [PubMed: 33291470]
12. Badar F, Xia Y. The interface region between articular cartilage and bone by μMRI and PLM at microscopic resolutions. Microsc Res Tech. 2021.
13. Mahar R, Batool S, Badar F, Xia Y. Quantitative measurement of T2, T1ρ and T1 relaxation times in articular cartilage and cartilage-bone interface by SE and UTE imaging at microscopic resolution. J Magn Reson. 2018;297:76–85. [PubMed: 30366222]
14. Bae WC, Dwek JR, Znamirowski R, et al. Ultrashort Echo Time MR Imaging of Osteochondral Junction of the Knee at 3 T: Identification of Anatomic Structures Contributing to Signal Intensity. Radiology. 2010;254(3):837–845. [PubMed: 20177096]
15. Xue YP, Ma YJ, Wu M, et al. Quantitative 3D Ultrashort Echo Time Magnetization Transfer Imaging for Evaluation of Knee Cartilage Degeneration In Vivo. J Magn Reson Imaging. 2021;54(4):1294–1302. [PubMed: 33894091]
16. Vanwanseele B, Eckstein F, Knecht H, Stüssi E, Spaepen A. Knee cartilage of spinal cord-injured patients displays progressive thinning in the absence of normal joint loading and movement. Arthritis Rheum. 2002;46(8):2073–2078. [PubMed: 12209511]
17. Shepherd DET, Seedhom BB. Thickness of human articular cartilage in joints of the lower limb. Annals of the Rheumatic Diseases. 1999;58(1):27–34. [PubMed: 10343537]
18. Kurrat HJ, Oberländer W. The thickness of the cartilage in the hip joint. J Anat. 1978 May;126(Pt 1):145–55. [PubMed: 649495]
19. Meachim G Effect of age on the thickness of adult articular cartilage at he shoulder joint. Ann Rheum Dis. 1971 Jan;30(1):43–6. doi: 10.1136/ard.30.1.43. [PubMed: 5548442]
20. Graichen H, Jakob J, von Eisenhart-Rothe R, Englmeier KH, Reiser M, Eckstein F. Validation of cartilage volume and thickness measurements in the human shoulder with quantitative magnetic resonance imaging. Osteoarthritis Cartilage. 2003 Jul;11(7):475–82. doi: 10.1016/s1063-4584(03)00077-3. [PubMed: 12814610]
21. Sophia Fox AJ, Bedi A, Rodeo SA. The basic science of articular cartilage: structure, composition, and function. Sports Health. 2009;1(6):461–468. [PubMed: 23015907]
22. Quinn TM, Häuselmann HJ, Shintani N, Hunziker EB. Cell and matrix morphology in articular cartilage from adult human knee and ankle joints suggests depth-associated adaptations to biomechanical and anatomical roles. Osteoarthritis Cartilage. 2013;21(12):1904–1912. [PubMed: 24455780]
23. Poole AR, Pidoux I, Reiner A, Rosenberg L. An immunoelectron microscope study of the organization of proteoglycan monomer, link protein, and collagen in the matrix of articular cartilage. J Cell Biol. 1982;93(3):921–937. [PubMed: 7119005]
24. Cheng KY, Lombardi AF, Chang EY, Chung CB. Knee Cartilage Imaging. Clin Sports Med. 2021;40(4):677–692. [PubMed: 34509205]
25. Mente PL, Lewis JL. Elastic modulus of calcified cartilage is an order of magnitude less than that of subchondral bone. J Orthop Res. 1994;12(5):637–647. [PubMed: 7931780]
26. Pedersen DR, Goetz JE, Kurriger GL, Martin JA. Comparative digital cartilage histology for human and common osteoarthritis models. Orthop Res Rev. 2013 Feb 12;2013(5):13–20. doi: 10.2147/ORR.S38400. [PubMed: 24465137]

Author Manuscript Author Manuscript Author Manuscript Author Manuscript

27. Hargrave-Thomas EJ, Thambyah A. The micro and ultrastructural anatomy of bone spicules found in the osteochondral junction of bovine patellae with early joint degeneration. J Anat. 2021 Dec;239(6):1452–1464. doi: 10.1111/joa.13518. Epub 2021 Jul 20. [PubMed: 34289114]
28. Clark JM, Huber JD. The structure of the human subchondral plate. The Journal of bone and joint surgery British volume. 1990;72 5:866–873. [PubMed: 2211774]
29. Walsh DA, McWilliams DF, Turley MJ, et al. Angiogenesis and nerve growth factor at the osteochondral junction in rheumatoid arthritis and osteoarthritis. Rheumatology (Oxford). 2010;49(10):1852–1861. [PubMed: 20581375]
30. Oegema TR Jr., Carpenter RJ, Hofmeister F, Thompson RC Jr. The interaction of the zone of calcified cartilage and subchondral bone in osteoarthritis. Microsc Res Tech. 1997;37(4):324–332. [PubMed: 9185154]
31. Arjmandi M, Kelly P, Thambyah A. The mechanical influence of bone spicules in the osteochondral junction: A finite element modelling study. Biomechanics and Modeling in Mechanobiology. 2021;20(6):2335–2351. [PubMed: 34468916]
32. Li G, Yin J, Gao J, et al. Subchondral bone in osteoarthritis: insight into risk factors and microstructural changes. Arthritis research & therapy. 2013;15(6):1–12.
33. Lawless BM, Sadeghi H, Temple DK, Dhaliwal H, Espino DM, Hukins DWL. Viscoelasticity of articular cartilage: Analysing the effect of induced stress and the restraint of bone in a dynamic environment. J Mech Behav Biomed Mater. 2017;75:293–301. [PubMed: 28763685]
34. Buckwalter J, Mankin H. Articular cartilage: tissue design and chondrocyte-matrix interactions. Instructional course lectures. 1998;47:477–486. [PubMed: 9571449]
35. The Osteochondral Junction. In: Thambyah A, Broom ND, eds. The Soft–Hard Tissue Junction: Structure, Mechanics and Function. Cambridge: Cambridge University Press; 2018:42–83.
36. Suri S, Walsh DA. Osteochondral alterations in osteoarthritis. Bone. 2012;51(2):204–211. [PubMed: 22023932]
37. Henkelman RM, Stanisz GJ, Graham SJ. Magnetization transfer in MRI: a review. NMR Biomed. 2001;14(2):57–64. [PubMed: 11320533]
38. Robson MD, Gatehouse PD, Bydder M, Bydder GM. Magnetic resonance: an introduction to ultrashort TE (UTE) imaging. J Comput Assist Tomogr. 2003;27(6):825–846. [PubMed: 14600447]
39. Du J, Carl M, Bae WC, et al. Dual inversion recovery ultrashort echo time (DIR-UTE) imaging and quantification of the zone of calcified cartilage (ZCC). Osteoarthritis Cartilage. 2013;21(1):77–85. [PubMed: 23025927]
40. Weiger M, Brunner DO, Dietrich BE, Müller CF, Pruessmann KP. ZTE imaging in humans. Magnetic resonance in medicine. 2013;70(2):328–332. [PubMed: 23776142]
41. Hafner S Fast imaging in liquids and solids with the Back-projection Low Angle ShoT (BLAST) technique. Magnetic resonance imaging. 1994;12(7):1047–1051. [PubMed: 7997092]
42. Ljungberg E, Damestani NL, Wood TC, et al. Silent zero TE MR neuroimaging: Current state-of-the-art and future directions. Progress in Nuclear Magnetic Resonance Spectroscopy. 2021;123:73–93. [PubMed: 34078538]
43. Bae WC, Biswas R, Chen K, Chang EY, Chung CB. UTE MRI of the Osteochondral Junction. Curr Radiol Rep. 2014 Feb 1;2(2):35. doi: 10.1007/s40134-013-0035-7. [PubMed: 25061547]
44. Brossmann J, Frank LR, Pauly JM, et al. Short echo time projection reconstruction MR imaging of cartilage: comparison with fat-suppressed spoiled GRASS and magnetization transfer contrast MR imaging. Radiology. 1997;203(2):501–507. [PubMed: 9114112]
45. Gold GE, Thedens DR, Pauly JM, et al. MR imaging of articular cartilage of the knee: new methods using ultrashort TEs. AJR Am J Roentgenol. 1998;170(5):1223–1226. [PubMed: 9574589]
46. Gatehouse PD, Bydder GM. Magnetic resonance imaging of short T2 components in tissue. Clin Radiol. 2003;58(1):1–19. [PubMed: 12565203]
47. Bergin CJ, Pauly JM, Macovski A. Lung parenchyma: projection reconstruction MR imaging. Radiology. 1991;179(3):777–781. [PubMed: 2027991]
48. Gold GE, Pauly JM, Macovski A, Herfkens RJ. MR spectroscopic imaging of collagen: tendons and knee menisci. Magn Reson Med. 1995;34(5):647–654. [PubMed: 8544684]

Author Manuscript Author Manuscript Author Manuscript Author Manuscript

49. Chen Y, Li L, Le N, Chang EY, Huang W, Ma YJ. On the fat saturation effect in quantitative ultrashort TE MR imaging. Magnetic Resonance in Medicine. 2022.
50. Springer F, Steidle G, Martirosian P, et al. Quick water-selective excitation of fast relaxing tissues with 3D UTE sequences. Magnetic Resonance in Medicine. 2014;71(2):534–543. [PubMed: 23440968]
51. Ma YJ, Jerban S, Jang H, Chang EY, Du J. Fat suppression for ultrashort echo time imaging using a novel soft-hard composite radiofrequency pulse. Magn Reson Med. 2019;82(6):2178–2187. [PubMed: 31317565]
52. Jang H, Carl M, Ma Y, et al. Fat suppression for ultrashort echo time imaging using a single-point Dixon method. NMR Biomed. 2019;32(5):e4069. [PubMed: 30768813]
53. Du J, Takahashi AM, Bae WC, Chung CB, Bydder GM. Dual inversion recovery, ultrashort echo time (DIR UTE) imaging: creating high contrast for short-T(2) species. Magn Reson Med. 2010;63(2):447–455. [PubMed: 20099332]
54. Gatehouse PD, Thomas RW, Robson MD, Hamilton G, Herlihy AH, Bydder GM. Magnetic resonance imaging of the knee with ultrashort TE pulse sequences. Magn Reson Imaging. 2004;22(8):1061–1067. [PubMed: 15527992]
55. Rahmer J, Blume U, Börnert P. Selective 3D ultrashort TE imaging: comparison of “dual-echo” acquisition and magnetization preparation for improving short-T 2 contrast. Magnetic Resonance Materials in Physics, Biology and Medicine. 2007;20(2):83–92.
56. Larson PE, Conolly SM, Pauly JM, Nishimura DG. Using adiabatic inversion pulses for long-T2 suppression in ultrashort echo time (UTE) imaging. Magnetic Resonance in Medicine: An Official Journal of the International Society for Magnetic Resonance in Medicine. 2007;58(5):952–961.
57. Cai Z, Wei Z, Wu M, et al. Knee osteochondral junction imaging using a fast 3D T(1)-weighted ultrashort echo time cones sequence at 3T. Magn Reson Imaging. 2020;73:76–83. [PubMed: 32828984]
58. Ma YJ, Jerban S, Carl M, et al. Imaging of the region of the osteochondral junction (OCJ) using a 3D adiabatic inversion recovery prepared ultrashort echo time cones (3D IR-UTE-cones) sequence at 3 T. NMR Biomed. 2019;32(5):e4080. [PubMed: 30794338]
59. Lombardi AF, Jang H, Wei Z, et al. High-contrast osteochondral junction imaging using a 3D dual adiabatic inversion recovery-prepared ultrashort echo time cones sequence. NMR Biomed. 2021;34(8):e4559. [PubMed: 34021649]
60. Shakoor D, Guermazi A, Kijowski R, et al. Diagnostic Performance of Three-dimensional MRI for Depicting Cartilage Defects in the Knee: A Meta-Analysis. Radiology. 2018;289(1):71–82. [PubMed: 30015587]
61. Du J, Bydder M, Takahashi AM, Carl M, Chung CB, Bydder GM. Short T2 contrast with three-dimensional ultrashort echo time imaging. Magnetic Resonance Imaging. 2011;29(4):470–482. [PubMed: 21440400]
62. Mackay JW, Low SB, Houston GC, Toms AP. Ultrashort TE evaluation of the osteochondral junction in vivo: a feasibility study. Br J Radiol. 2016;89(1059):20150493. [PubMed: 26781345]
63. Kaggie JD, Markides H, Graves MJ, et al. Ultra Short Echo Time MRI of Iron-Labelled Mesenchymal Stem Cells in an Ovine Osteochondral Defect Model. Scientific Reports. 2020;10(1):8451. [PubMed: 32439838]
64. Chu CR, Williams AA, West RV, et al. Quantitative Magnetic Resonance Imaging UTE-T2* Mapping of Cartilage and Meniscus Healing After Anatomic Anterior Cruciate Ligament Reconstruction. Am J Sports Med. 2014;42(8):1847–1856. [PubMed: 24812196]
65. Titchenal MR, Williams AA, Chehab EF, et al. Cartilage Subsurface Changes to Magnetic Resonance Imaging UTE-T2* 2 Years After Anterior Cruciate Ligament Reconstruction Correlate With Walking Mechanics Associated With Knee Osteoarthritis. Am J Sports Med. 2018;46(3):565–572. [PubMed: 29293364]
66. Cerejo R, Dunlop DD, Cahue S, Channin D, Song J, Sharma L. The influence of alignment on risk of knee osteoarthritis progression according to baseline stage of disease. Arthritis & Rheumatism. 2002;46(10):2632–2636. [PubMed: 12384921]

Author Manuscript Author Manuscript Author Manuscript Author Manuscript

67. Chehab EF, Favre J, Erhart-Hledik JC, Andriacchi TP. Baseline knee adduction and flexion moments during walking are both associated with 5 year cartilage changes in patients with medial knee osteoarthritis. Osteoarthritis and cartilage. 2014;22(11):1833–1839. [PubMed: 25211281]
68. Mündermann A, Dyrby CO, Andriacchi TP. Secondary gait changes in patients with medial compartment knee osteoarthritis: increased load at the ankle, knee, and hip during walking. Arthritis & rheumatism. 2005;52(9):2835–2844. [PubMed: 16145666]
69. Williams AA, Erhart-Hledik JC, Asay JL, et al. Patient-Reported Outcomes and Knee Mechanics Correlate With Patellofemoral Deep Cartilage UTE-T2* 2 Years After Anterior Cruciate Ligament Reconstruction. Am J Sports Med. 2021;49(3):675–683. [PubMed: 33507800]
70. Shao H, Chang EY, Pauli C, et al. UTE bi-component analysis of T2* relaxation in articular cartilage. Osteoarthritis Cartilage. 2016;24(2):364–373. [PubMed: 26382110]
71. Alecio F Lombardi ZW, Dina Moazamian, Saeed Jerban, Hyungseok Jang, Nicole Le JD, Christine Chung, Chang Eric Y., Ya-Jun Ma. Quantitative Ultrashort Echo Time (UTE) imaging of Osteochondral Junction. Abrstract from the International Magnetic Resonance in Medicine Meeting. 2022.
72. Liu J, Wei Y, Ma YJ, Zhu YC, Zhou Q, Zhao YH. Magnetic resonance imaging of the zone of calcified cartilage in the knee joint using 3-dimensional ultrashort echo time cones sequences. Chin Med J (Engl). 2019;132(5):562–568. [PubMed: 30807355]
73. Posadzy M, Desimpel J, Vanhoenacker F. Staging of Osteochondral Lesions of the Talus: MRI and Cone Beam CT. J Belg Soc Radiol. 2017;101(Suppl 2):1.
74. Jang H, Ma Y, Carl M, Lombardi AF, Chang EY, Du J. Feasibility of an Inversion Recovery-Prepared Fat-Saturated Zero Echo Time Sequence for High Contrast Imaging of the Osteochondral Junction. Frontiers in Endocrinology. 2021;12.
75. Rautiainen J, Lehto LJ, Tiitu V, et al. Osteochondral Repair: Evaluation with Sweep Imaging with Fourier Transform in an Equine Model. Radiology. 2013;269(1):113–121. [PubMed: 23674789]
76. Idiyatullin D, Corum C, Park JY, Garwood M. Fast and quiet MRI using a swept radiofrequency. J Magn Reson. 2006;181(2):342–349. [PubMed: 16782371]
77. Nykänen O, Leskinen HPP, Finnilä MAJ, et al. Bright ultrashort echo time SWIFT MRI signal at the steochondral junction is not located in the calcified cartilage. J Orthop Res. 2020;38(12):2649–2656. [PubMed: 32543707]
78. Guermazi A, Roemer FW, Alizai H, et al. State of the Art: MR Imaging after Knee Cartilage Repair Surgery. Radiology. 2015;277(1):23–43. [PubMed: 26402492]
79. Battaglia M, Rimondi E, Monti C, et al. Validity of T2 mapping in characterization of the regeneration tissue by bone marrow derived cell transplantation in osteochondral lesions of the ankle. European Journal of Radiology. 2011;80(2):e132–e139. [PubMed: 20801594]
80. Rehnitz C, Kuni B, Wuennemann F, et al. Delayed gadolinium-enhanced MRI of cartilage (dGEMRIC) and T2 mapping of talar osteochondral lesions: Indicators of clinical outcomes. Journal of Magnetic Resonance Imaging. 2017;46(6):1601–1610. [PubMed: 28419612]
81. Rizzo G, Cristoforetti A, Marinetti A, et al. Quantitative MRI T2 Mapping Is Able to Assess Tissue Quality After Reparative and Regenerative Treatments of Osteochondral Lesions of the Talus. Journal of Magnetic Resonance Imaging. 2021;54(5):1572–1582. [PubMed: 34047400]
82. Wang N, Mirando AJ, Cofer G, Qi Y, Hilton MJ, Johnson GA. Characterization complex collagen fiber architecture in knee joint using high-resolution diffusion imaging. Magn Reson Med. 2020;84(2):908–919. [PubMed: 31962373]
83. Tyler DJ, Robson MD, Henkelman RM, Young IR, Bydder GM. Magnetic resonance imaging with ultrashort TE (UTE) PULSE sequences: technical considerations. Journal of Magnetic Resonance Imaging: An Official Journal of the International Society for Magnetic Resonance in Medicine. 2007;25(2):279–289.
84. Carl M, Bydder GM, Du J. UTE imaging with simultaneous water and fat signal suppression using a time-efficient multispoke inversion recovery pulse sequence. Magn Reson Med. 2016;76(2):577–582. [PubMed: 26309221]

Author Manuscript Author Manuscript Author Manuscript Author Manuscript

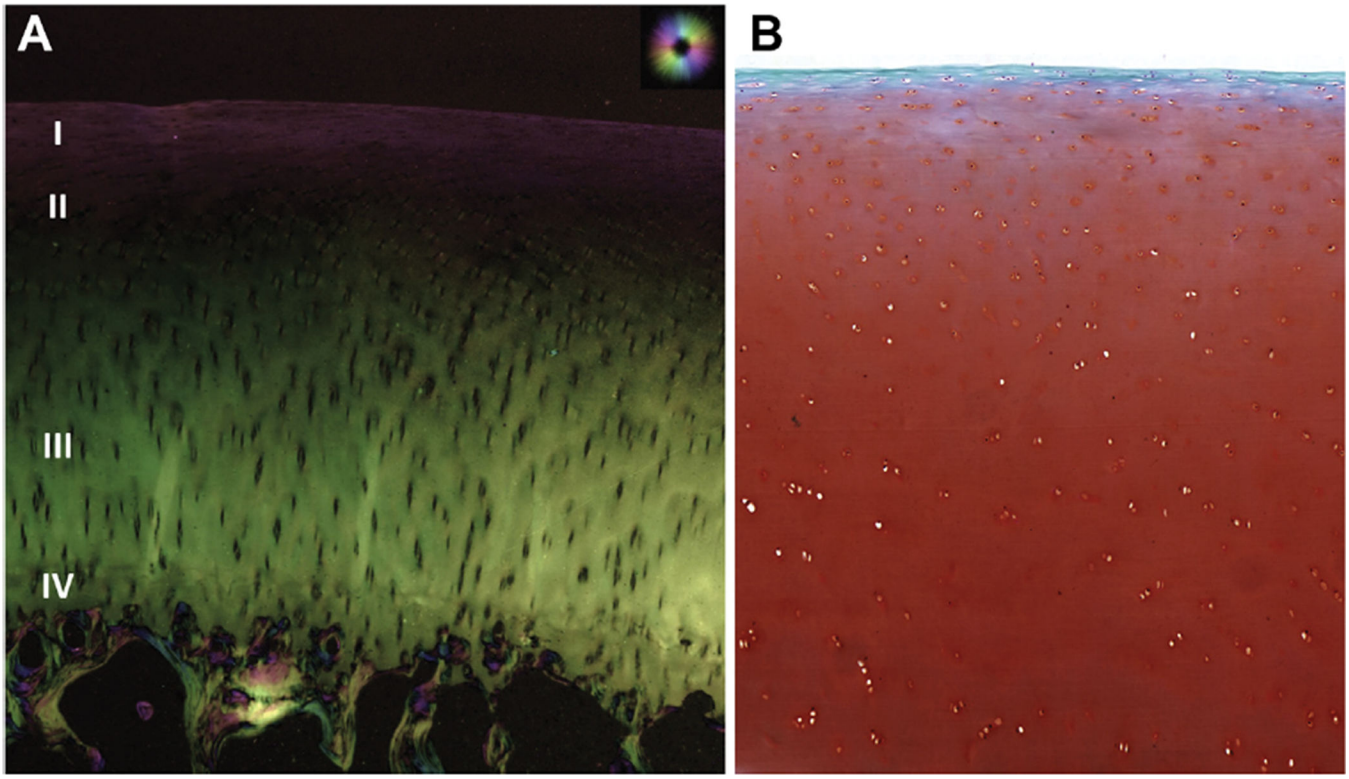

Fig. 1.

Normal histologic appearance of cartilage. (A) Quantitative polarization image with color representing collagen fiber orientation (color wheel in the upper right) and brightness representing retardance. Collagen fiber orientation varies between 60° to 90° when compared between zones I and III. Zone II shows lower intensity, reflecting relative fiber disorganization. Note that chondrocyte density decreases with increasing depth. (B) Photomicrograph of Safranin-O-stained slide shows normal proteoglycan distribution, with the strongest concentration at the deepest zone and lowest concentration more superficially. Zone I: Superficial, Zone II: Transitional, Zone III: Radial, Zone IV: calcified. Image reproduced with permission from Cheng et al.[24].

Author Manuscript Author Manuscript Author Manuscript Author Manuscript

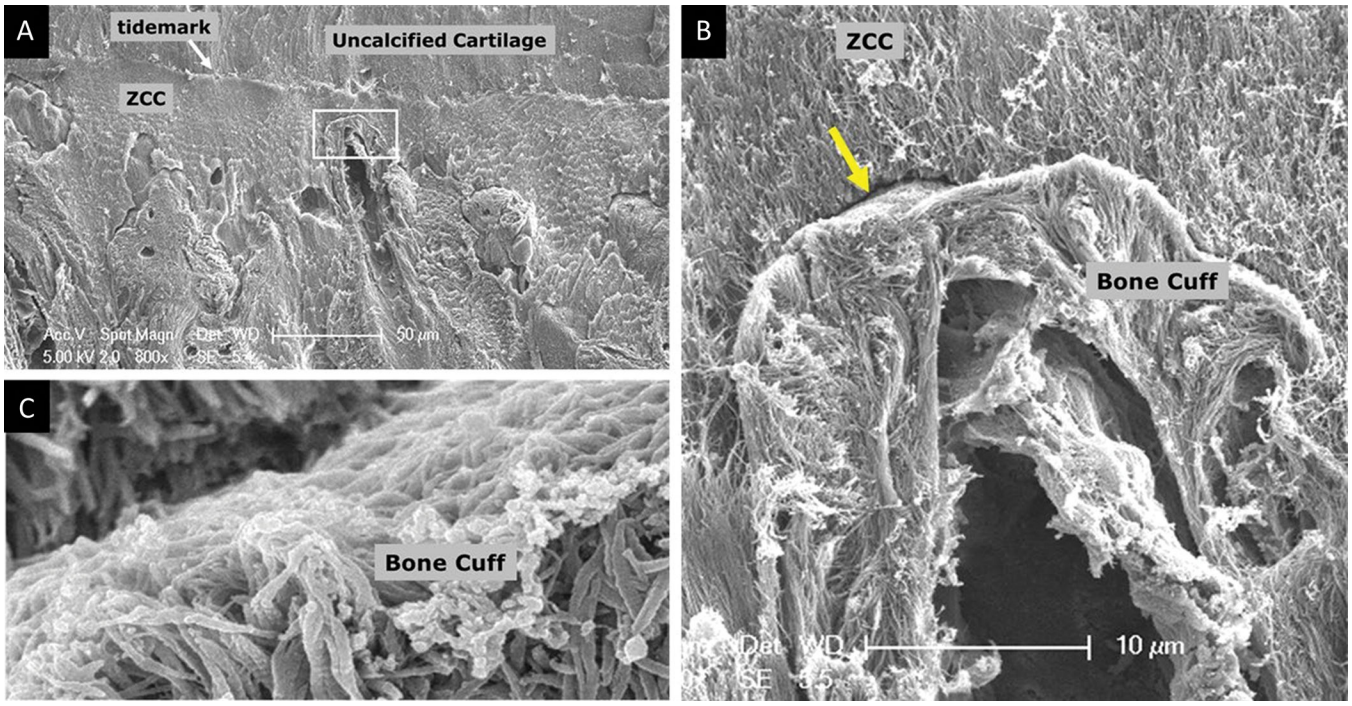

Fig 2.

(A) SEM image of the uncalcified cartilage ZCC bone region. The high magnification image for the box region in A highlights the tip or apex of a bone spicule (B). The gap between ZCC and bone cuff is indicated by a yellow arrow in B and highlighted with high resolution (C). Image reproduced with permission from Hargrave-Thomas et al.[27].

Author Manuscript Author Manuscript Author Manuscript Author Manuscript

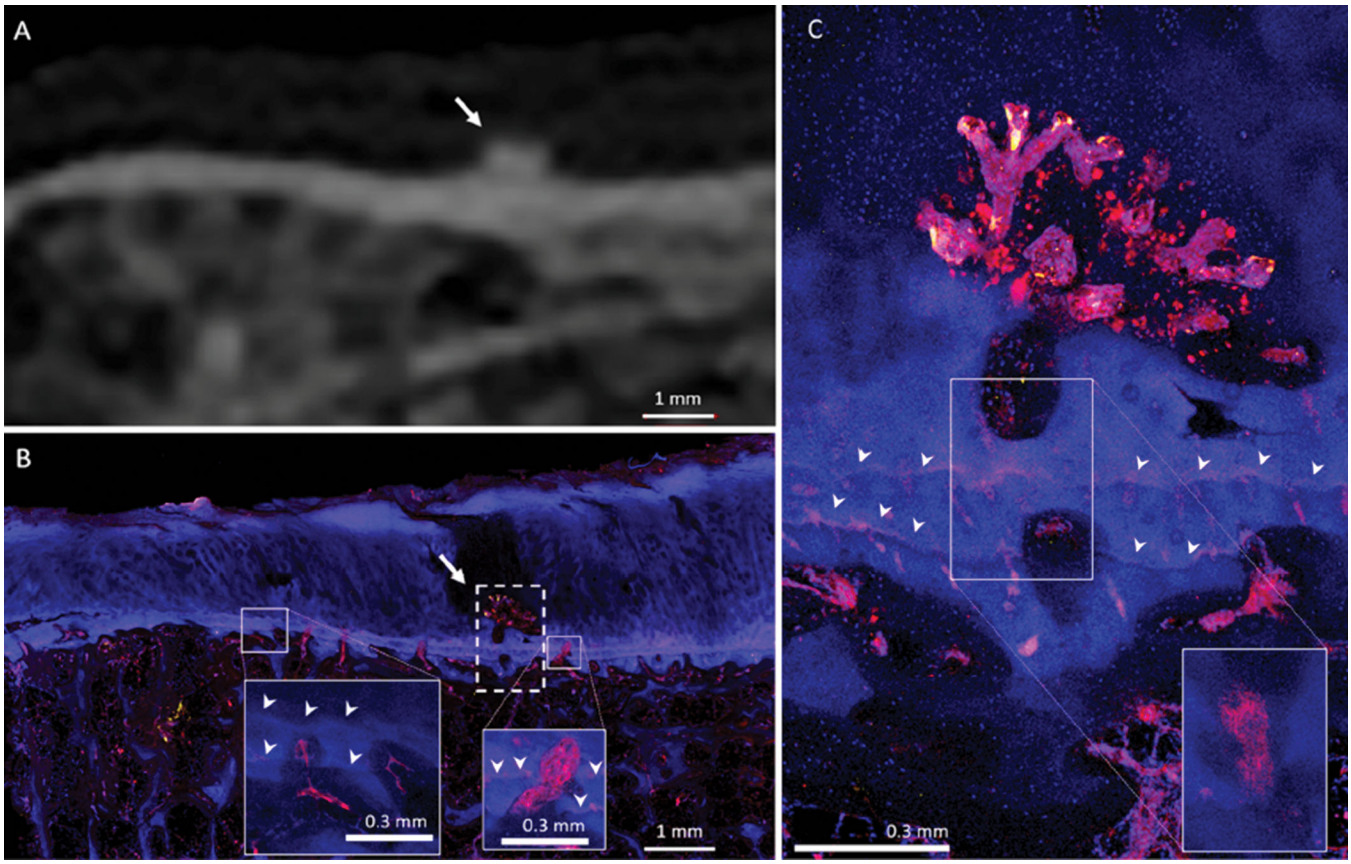

Fig 3.

Medial tibial plateau containing a small high-density mineralized protrusion (HDMP). (A) CT image shows mesa-like HDMP (arrow) with associated subchondral bone plate thickening. (B) The micrograph in the same location as Figure 2A shows HDMP associated with the calcified cartilage (arrow), exhibiting superficial vascular invasion and cartilage degeneration in the dotted-boxed area. Vascular channels are present at the OCJ throughout the tissue (e.g., solid boxed and inset). Distant from the HDMP, channels tend to terminate within the calcified cartilage, but near the HDMP, they more frequently cross all tidemarks (arrowheads). Insets are subsets of the full z-stack of confocal optical planes, which allows the identification of some channels not otherwise apparent in a full-stack maximum-intensity projection (large image). (C) Enlarged image of the boxed area in Figure 2B. A fluorescent protrusion extends above both tidemarks (arrowheads) and is highly vascularized at its superficial margin, where endothelial (UEA-I, red), TRAP-positive (TRAP activity, yellow), and other cells (DAPI-stained nuclei, blue) form organized structures. The boxed area shows the inset at the same scale observed within a subset of optical planes, revealing the uninterrupted tortuous path of the large vascular channel leading to the HDMP. HDMP: high-density mineralized protrusions. Image reproduced with permission from Lombardi et al.[11].

Author Manuscript Author Manuscript Author Manuscript Author Manuscript

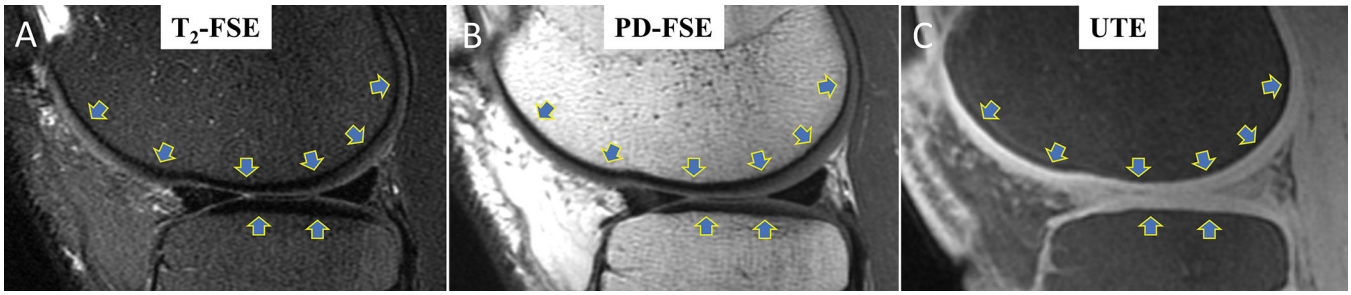

Fig 4.

Comparison between the normal appearance of cartilage on conventional MR and UTE MR sequences. Sagittal FSE T2-weighted (A) and PD-weighted (B) FSE MRI of the lateral compartment of the knee shows low signal intensity within the deep layers of cartilage and OCJ (arrows in A and B). Sagittal UTE MRI of the same knee region shows increased signal intensity across all layers of cartilage, including the OCJ represented by a bright line (arrows in C). However, the contrast between the superficial layers and the OCJ on the UTE MRI (C) is not optimal. This is why other techniques, such as IR-UTE and DIR-UTE, were later developed to increase the image contrast between superficial and deep layers of cartilage and facilitate the identification of the OCJ.

Author Manuscript Author Manuscript Author Manuscript Author Manuscript

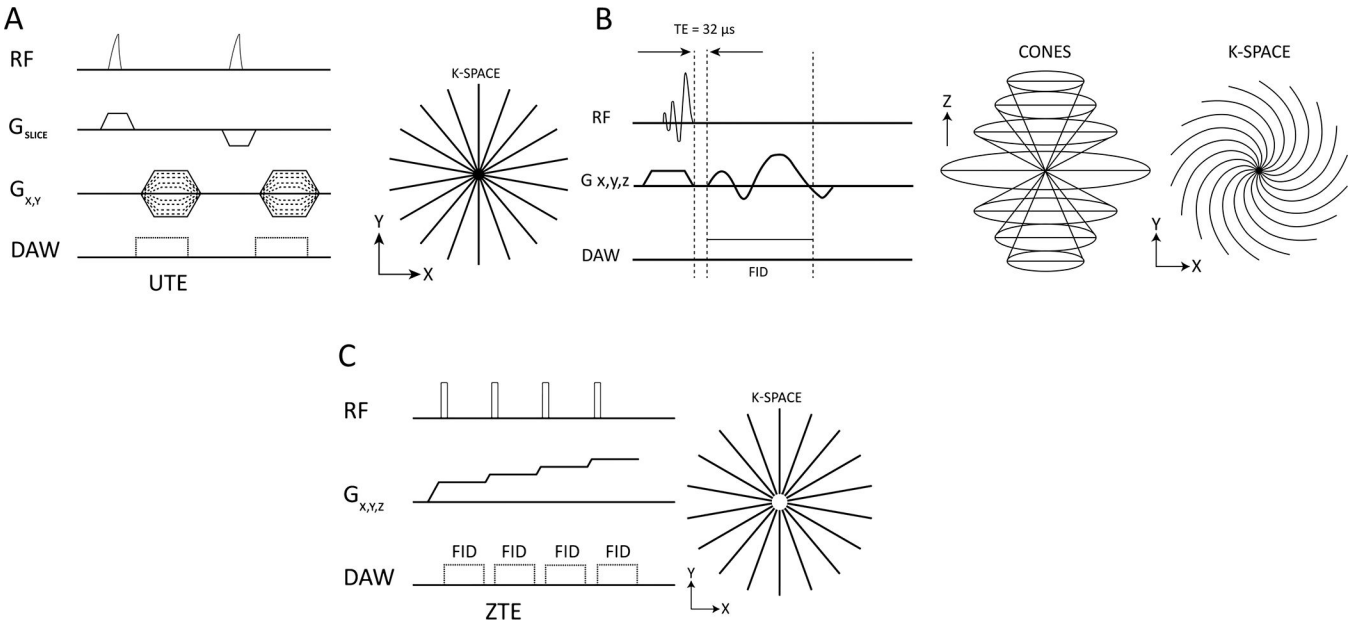

Fig 5.

(A) Basic 2D UTE sequence diagram. A half-soft RF pulse with VERSE design is applied together with a slice-selective gradient. After excitation, the spatial encoding gradient is turned on, and data acquisition begins with radial k-space sampling. The process is repeated with a gradient applied in the opposite direction. (B) 3D UTE cones sequence diagram. A short slab-selective RF pulse is used for signal excitation, followed by a Cones trajectory k-space sampling. (C) Basic ZTE sequence diagram. Here the RF pulse is applied with the gradient completely ramped up, and progressive small increments of gradients are subsequently applied for each of the remaining radiofrequency pulses, followed by a radial k-space sampling. As the RF pulse is applied with the gradients on, the center of the k-space has a small gap with some missing points that can be later recovered by mathematical reconstruction algorithms.

Author Manuscript Author Manuscript Author Manuscript Author Manuscript

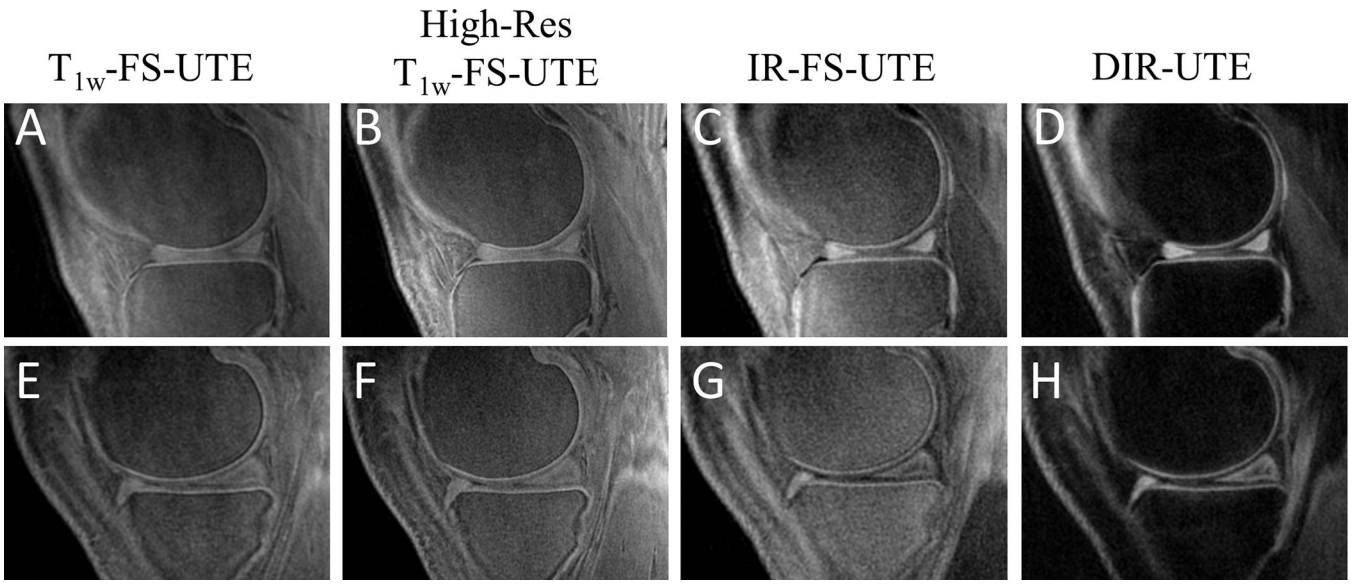

Fig 6.

Sagittal UTE MR images of the lateral (upper row) and medial (lower row) compartments of the knee of a healthy volunteer were scanned with four different UTE sequences: (A and E) T1-weighted fat-suppressed, (B and F) T1-weighted fat-suppressed with high resolution, (C and G) single adiabatic inversion recovery, and (D and H) dual adiabatic inversion recovery.

Author Manuscript Author Manuscript Author Manuscript Author Manuscript

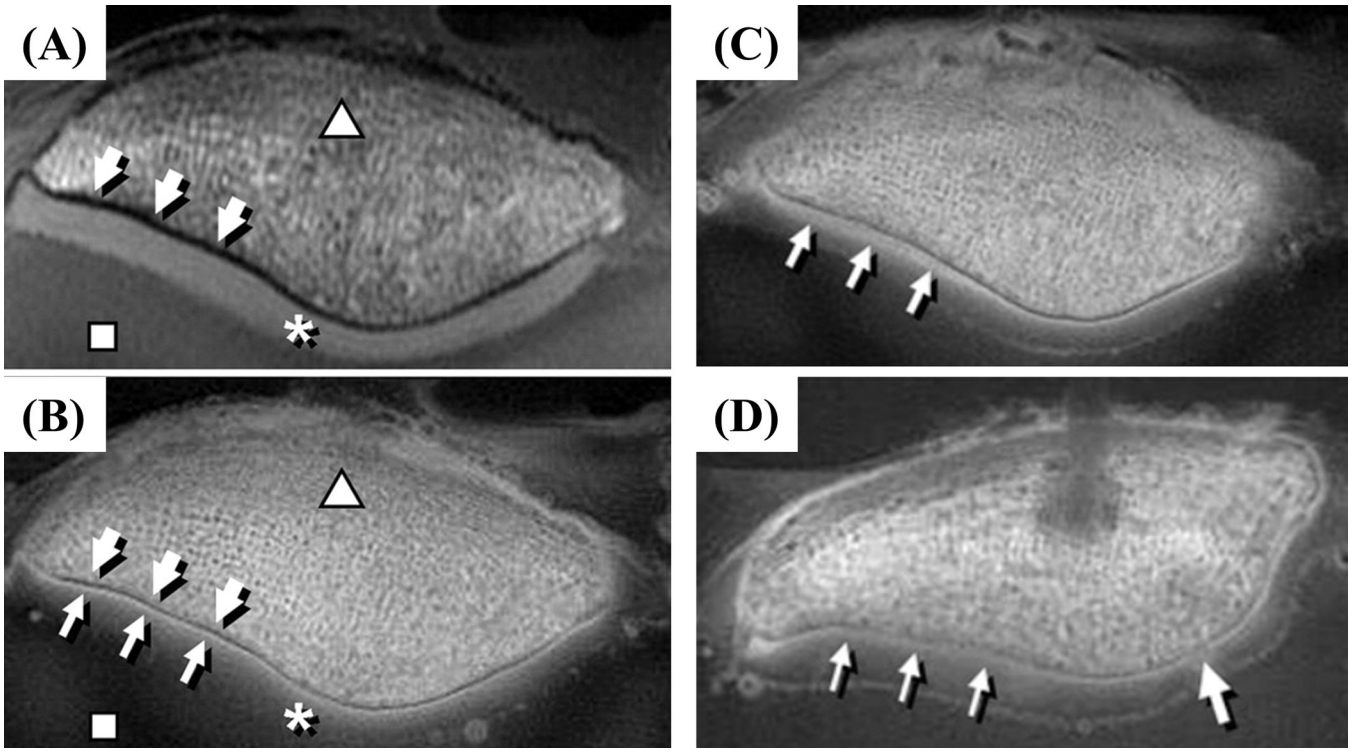

Fig 7.

MR imaging appearances in the axial plane of experimentally prepared samples suggested that both the deep layer of UCC and the layer of CC contribute to a high linear signal on DIR UTE images. A, DIR UTE image shows a characteristic pattern of high linear signal intensity (arrows) near the osteochondral junction of an untreated and intact sample. After this sample was divided into fragments (samples 1–4 in drawings above B–D), the characteristic pattern was present in, B, C, and D, untreated UCC-only samples (↑ [sample 1]), B, UCC/CC/bone samples (↓ [sample 2]), and, D, papain-treated CC/bone samples (↓ [sample 4]). The pattern was also present in, E, a surgically prepared CC/bone sample (↓ [sample 5]). The pattern was absent in, B, C, and D, superficial-to-middle layers of UCC-only samples (* [sample 1]) and, C, a region where UCC and CC were resected (○ [sample 3]). By deduction, both UCC and CC, but not subchondral bone, contribute to the pattern of signal. F–I, Histologic analysis of samples 2–5 show that our sample preparation successfully isolated intended components of osteochondral tissues: F, UCC/CC/bone sample consisted of all three components of bone (blue), CC (purple [↓]), and UCC (red). G, Resected region (○) consisted of mainly bone (blue) and small pockets of CC (↓). H, Papain-treated CC/bone sample consisted of bone and CC (↓) but not UCC. I, Surgically prepared CC/bone sample also consisted of bone and CC (↓) but not UCC in the defect region. Dotted lines signify magnification from the top row of micrographs. Image reproduced with permission from Bae et al.[14] and the Radiologic Society of North America.

Author Manuscript Author Manuscript Author Manuscript Author Manuscript

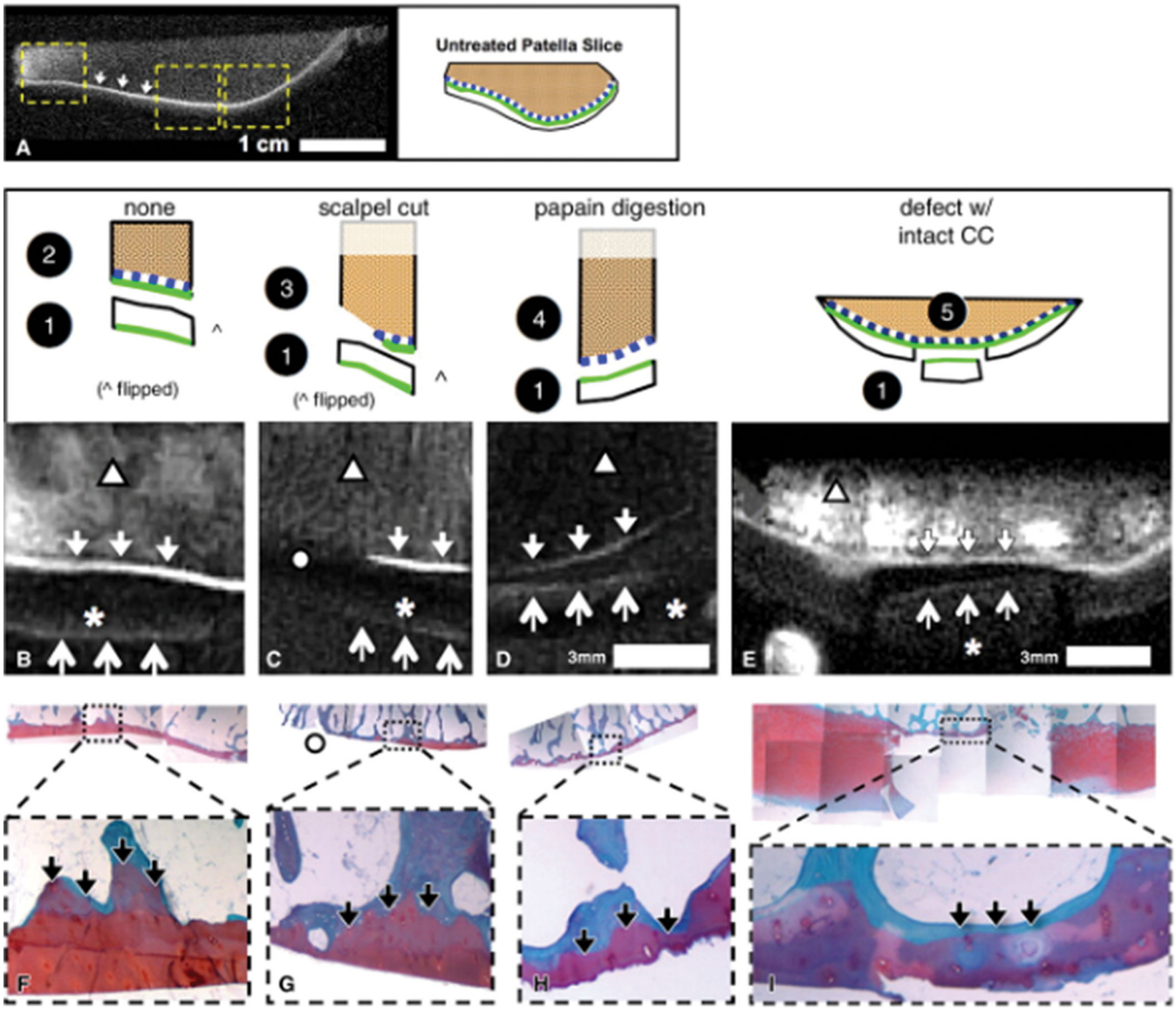

Fig 8.

MR images of a human patella in the axial plane obtained by using T1-weighted FSE (A) and UTE dual-echo subtraction (B-D). UTE MRI had a high-intensity linear signal near the osteochondral junction (thin arrows in B). A subset of patellar samples showed different UTE signal patterns near the osteochondral junction characterized by thickening of the linear signal (arrow in C) and diminution (thin arrows in D) or absence (thick arrow in D) of the signal. Note the ringing artifacts surrounding the signal of the osteochondral junction on UTE due to chemical shift artifacts from subchondral bone fat, which also have a relatively short T2* and, thus, present strong signal. Image reproduced with permission from Bae et al.[14] and the Radiologic Society of North America, including mild modifications from the original.

Author Manuscript Author Manuscript Author Manuscript Author Manuscript

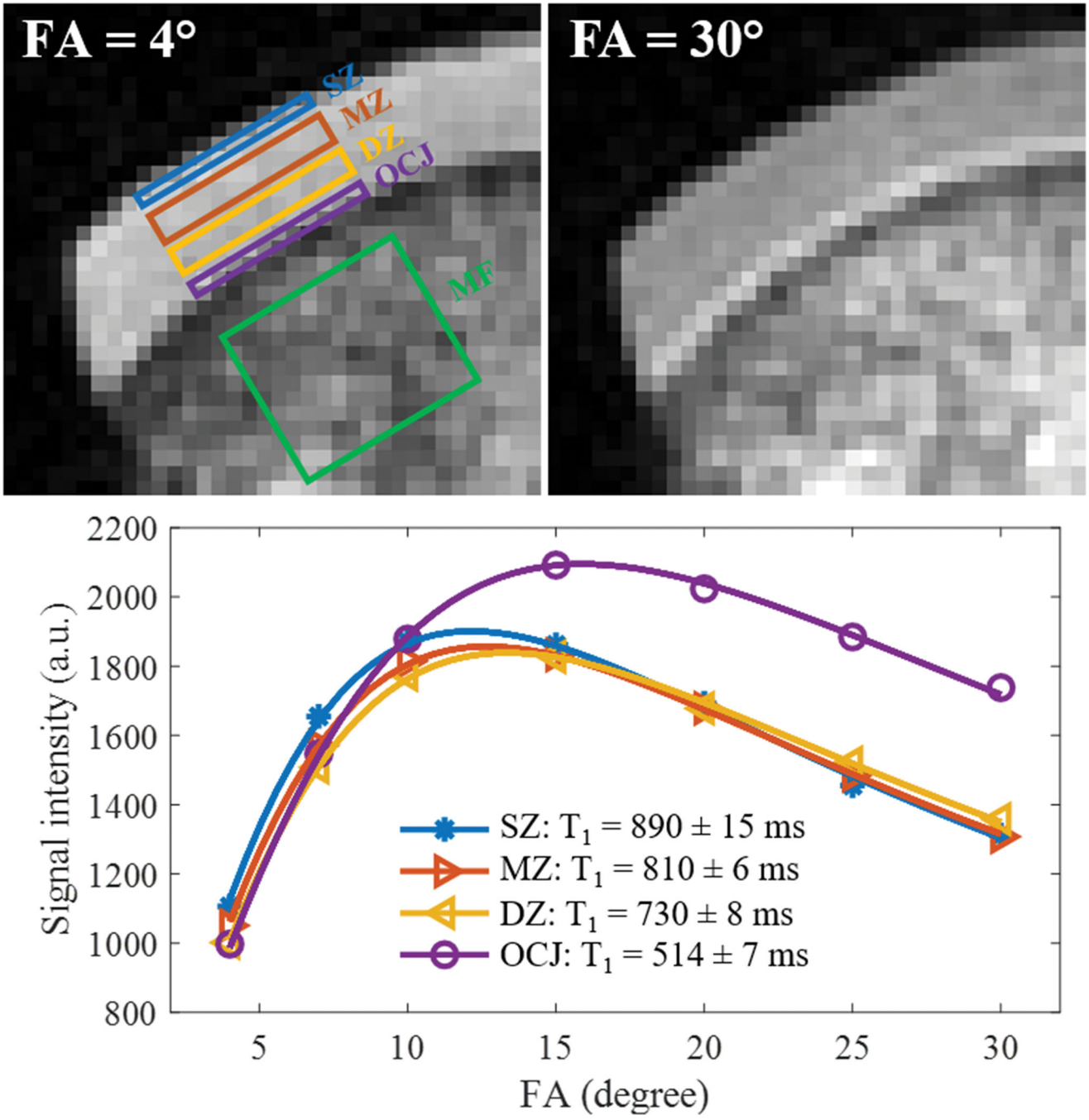

Fig 9.

T1 measurement for a patellar cartilage sample on the superficial zone (SZ), middle zone (MZ), deep zone (DZ), and OCJ region. The bone marrow fat (MF) region is also labeled in A. Images with flip angles of 4° and 30° are shown in A and B, respectively. A high signal intensity band can be seen in the OCJ region for the image with a flip angle of 30°. The fitting curves and T1 values for SZ, MZ, DZ, and OCJ are all shown in C. T1 value decreases gradually from the SZ to OCJ. Image reproduced with permission from Cai et al. [57].

Author Manuscript Author Manuscript Author Manuscript Author Manuscript

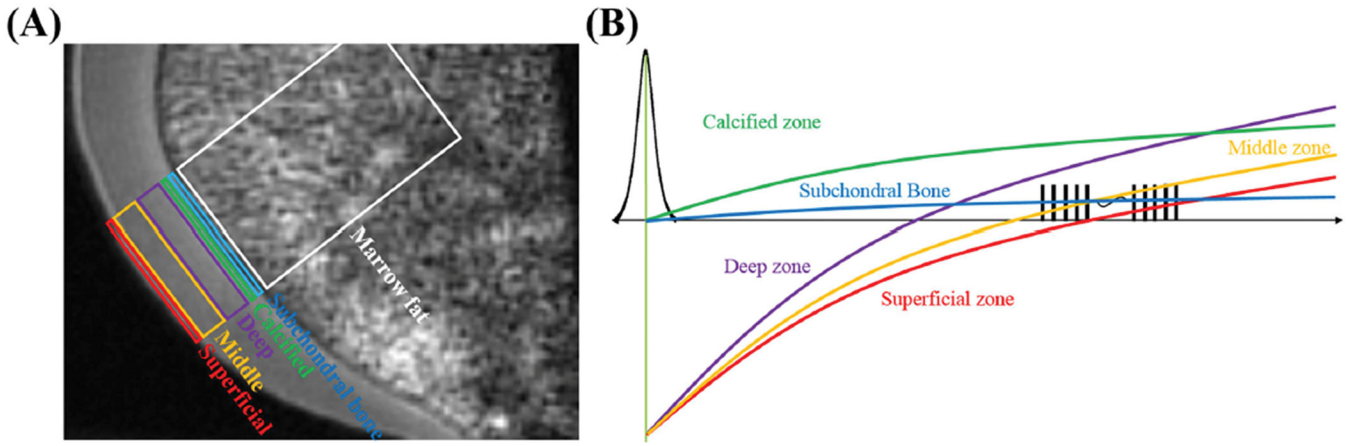

Fig 10.

The contrast mechanism for the OCJ region imaging using the 3D IR-FS-UTE-Cones sequence. Panel A depicts the regions of different cartilage layers (i.e., superficial, middle, deep, and calcified layers), subchondral bone, and marrow fat in patellar cartilage. The magnetizations of superficial, middle, and deep layers of uncalcified cartilage are inverted by the adiabatic IR pulse (B). In contrast, calcified layer cartilage and subchondral bone magnetizations are mostly saturated due to their short T2s. Thus, both the calcified layer cartilage and subchondral bone longitudinal magnetizations recover rapidly from zero after saturation. When TI is selected to suppress superficial zone cartilage, the calcified layers express a higher signal than the more superficial layer cartilages. Subchondral bone remains low signal due to its low proton density. Image reproduced with permission from Ma et al. [58].

Author Manuscript Author Manuscript Author Manuscript Author Manuscript

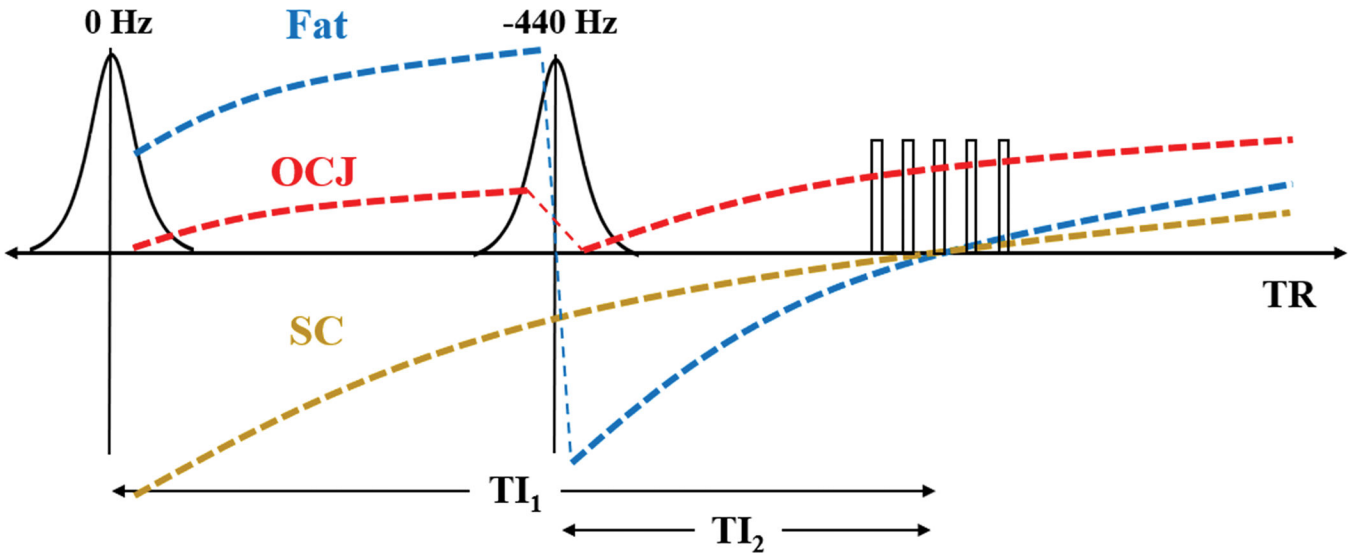

Fig 11.

Dual inversion recovery ultrashort echo time (DIR-UTE) sequence diagram. The DIR-UTE sequence utilizes two adiabatic IR pulses with center frequencies of 0 and 440 Hz (fat frequency offset at 3 T) to invert long T2 water and fat, respectively. These IR pulses have a relatively narrow bandwidth of around 500 Hz. TIs were determined experimentally to reach the nulling point at the same time as data acquisition. At the optimized TI1 and TI2 in this DIR-UTE sequence, superficial layers of cartilage (SC) and fat can both be suppressed simultaneously. The osteochondral junction (OCJ) signal was largely saturated when the second IR preparation pulse was applied due to its short T2 relaxation time compared with the relatively long relaxation times of the adiabatic IR pulses. The relatively high signals from the OCJ were acquired with a train of UTE spokes (i.e., 21 used in this study) at the signal nulling point of SC and fat. Hard pulse excitation was applied to reduce eddy current effects. Both RF and gradient spoiling were used for crushing the residual transverse magnetizations after acquisition in each UTE spoke. Image reproduced with permission from Lombardi et al. [59].

Author Manuscript Author Manuscript Author Manuscript Author Manuscript

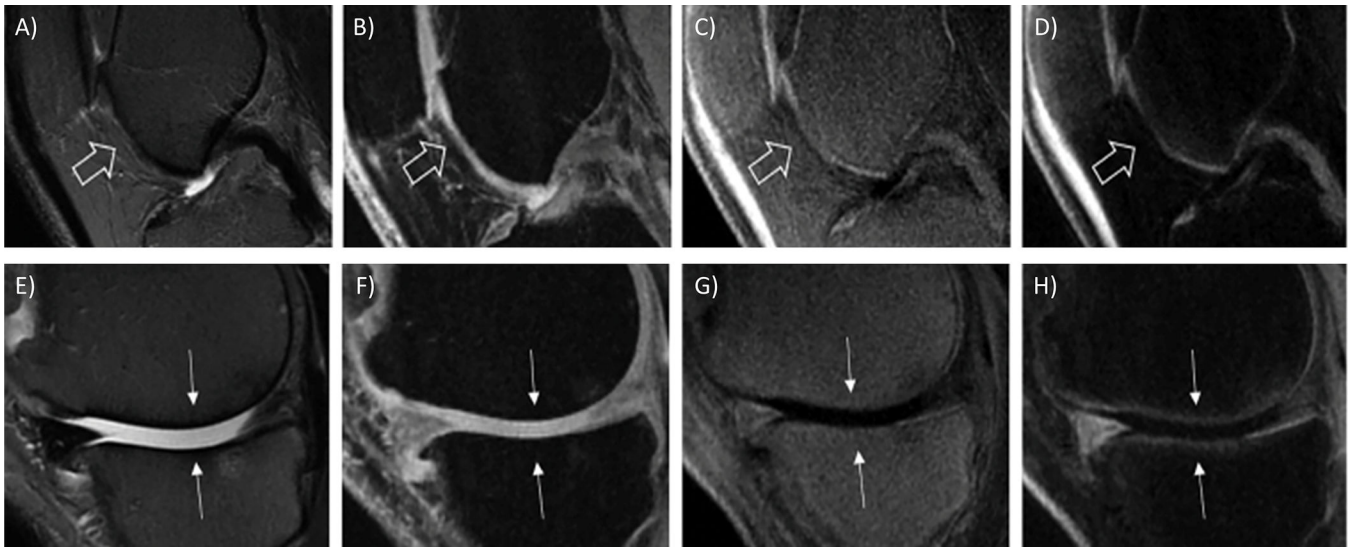

Fig 12.

Images from T2-weighted fast spin-echo (T2w-FSE) (A, B), fast spoiled gradient echo (FSPGR) (C, D), inversion recovery-fat suppression-ultrashort echo time (IR-FS-UTE) cones (E, F), and dual inversion recovery ultrashort echo time (DIR-UTE) cones (G, H) performed in the knees of two patients with osteoarthritis (the first row represents the first patient [50-year-old male] and the second row represents the second patient [48-year-old male]). Cartilage thinning can be seen on the weight-bearing area of the medial compartment in the first patient (indicated by arrows in A, C, E, G) and on the trochlea in the second patient (open arrows in B, D, F, H). Note the interruption of the bright line representing the osteochondral junction on both IR-FS-UTE cones and DIR-UTE cones images (E, F, G, H). The 3D DIR-UTE cones sequence (G and H) is more efficient in suppressing the subchondral bone fat than the IR-FS-UTE cones (E, F). Image reproduced with permission from Lombardi et al. [59].

Author Manuscript Author Manuscript Author Manuscript Author Manuscript

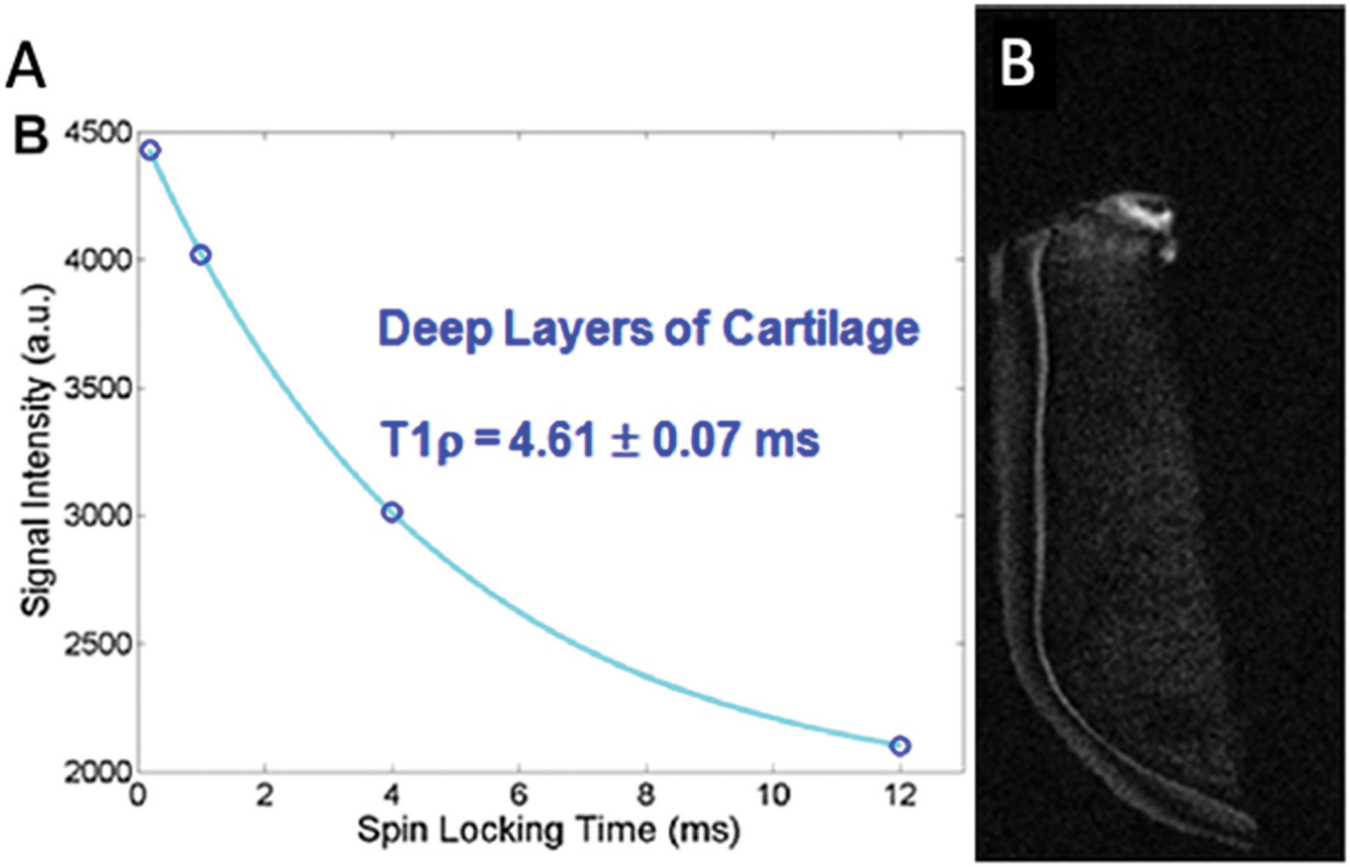

Fig 13.

Single component curve fitting shows a T1rho of 4.61 ± 0.07 ms (A) for the zone of calcified cartilage (ZCC) of the patella (bright line in B). Image reproduced with permission from Du et al.[39].

Author Manuscript Author Manuscript Author Manuscript Author Manuscript

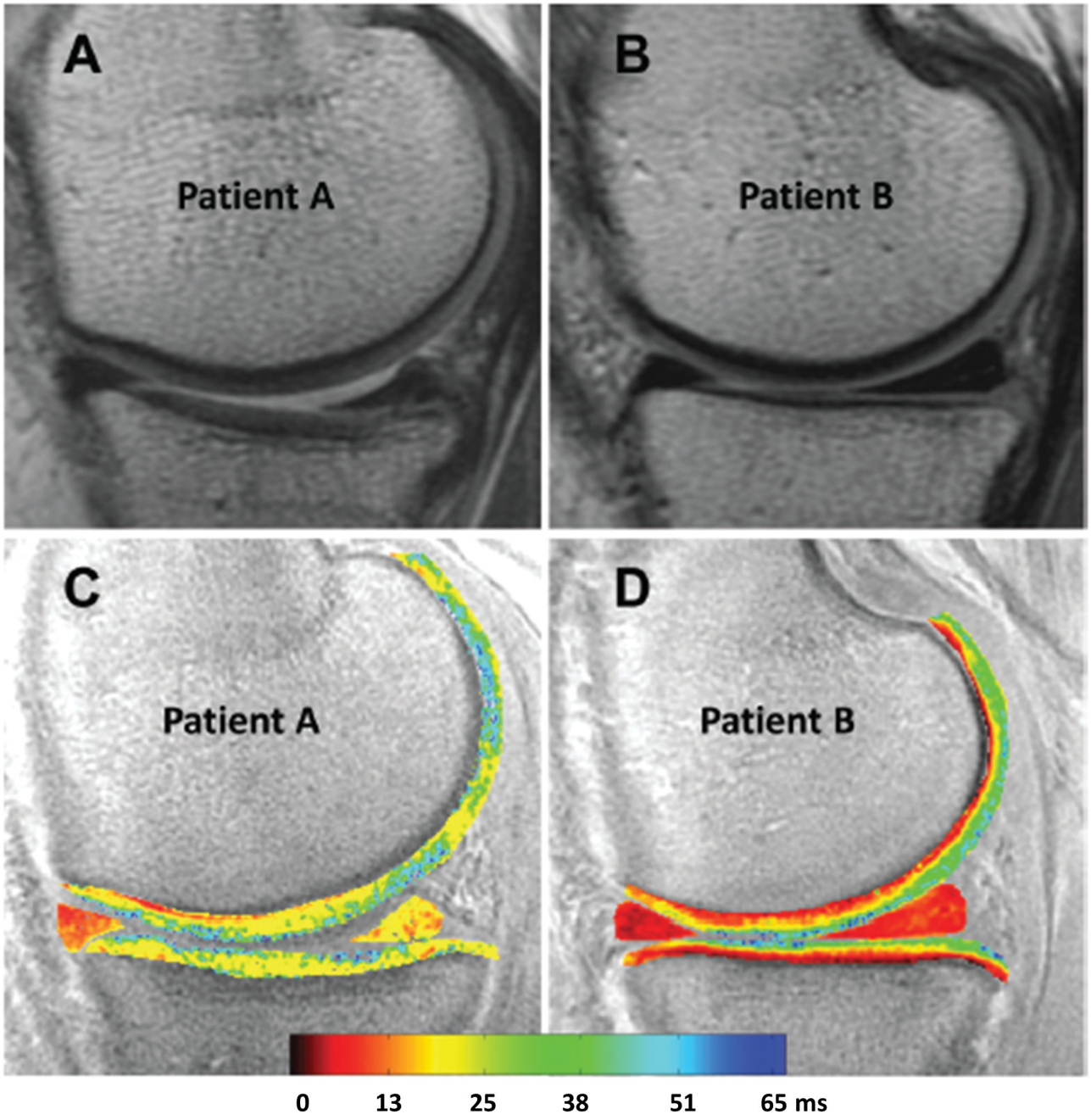

Fig 14.

Top: Morphological magnetic resonance imaging (sagittal proton density without fat saturation) of the medial compartment of the tibiofemoral joint of two anterior cruciate ligament–reconstructed patients: (A) 28-year-old female and (B) 27-year-old female. Both patients had Outerbridge grade 0 in the central and posterior medial femoral condyle and central medial tibial plateau regions of cartilage. Bottom: UTE-T2* maps of the same two patients. (C) The same patient from A had both high knee adduction moment (KAM) and high UTE-T2* values. (D) The same patient from B had both low KAM and low UTE-T2* values. Note that patient B demonstrates a similar laminar structure to articular cartilage

Author Manuscript Author Manuscript Author Manuscript Author Manuscript

as the uninjured participant (Figure 1), while patient A does not. Image reproduced with permission from Chu et al.[64].

Author Manuscript Author Manuscript Author Manuscript Author Manuscript

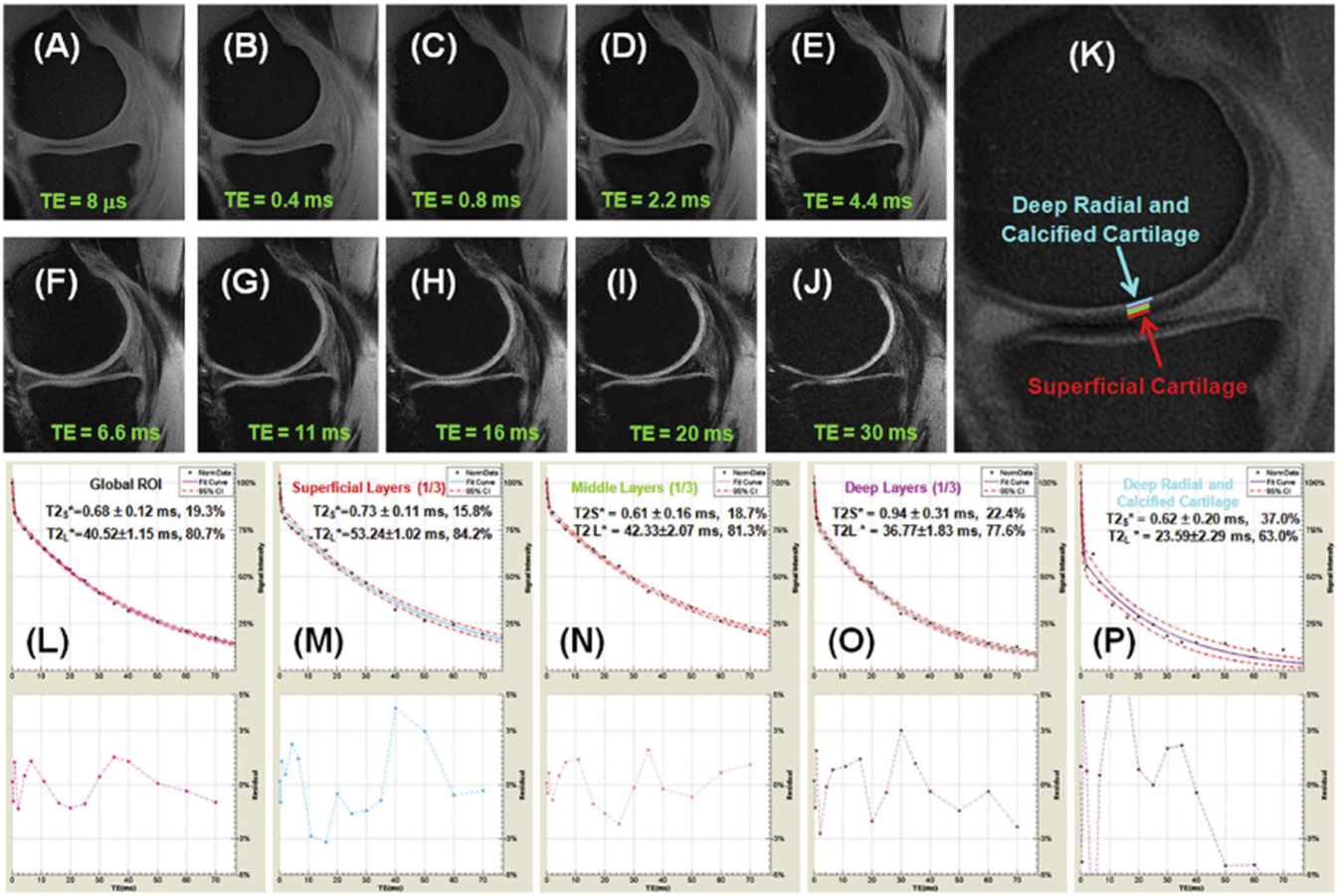

Fig 15.

UTE imaging of a 59-year-old volunteer who is a regular runner and in good health. Selected interleaved 4-echo UTE acquisitions with a TE of 8 μs (A), 0.4 ms (B), 0.8 ms (C), 2.2 ms (D), 4.4 ms (E), 6.6 ms (F), 11 ms (G), 16 ms (H), 20 ms (I), 30 ms (J), echo subtraction (K), and bi-component T2* analysis for the global ROI (L), superficial layer (M), middle layer (N), deep layer (O) and deep radial and calcified cartilage (P). The echo subtraction image was generated by subtracting the image with a TE of 2.2 ms from the first image with a TE of 8 μs. ROIs for the different layers of femoral cartilage were shown in (K). 95% fitting confidence level was displayed in UTE T2* bi-component analysis with n = 16. Image reproduced with permission from Shao et al.[70].

Author Manuscript Author Manuscript Author Manuscript Author Manuscript

Table 1.

Summary of the UTE techniques for morphological OCJ imaging

Technique/scanner	Subjects	Main findings	Ref.
High resolution 2D UTE with a TE of 150 μs/1.5T GE scanner	Human patellar samples	UTE imaging provided much better delineation of cartilage lesions compared with MT contrast and spoiled gradient-recalled acquisition in the steady state imaging.	44
High resolution 3D cones with a TE of 0.6 ms/1.5T GE scanner	Knee joints from healthy volunteers and patients with cartilage damage	3D cones sequence was suited to scan the whole knee cartilage with high resolution and isotropic multiplanar reconstruction showing cartilage damage as well as abnormalities in the deep layers and OCJ.	45
Dual-echo subtraction and magnetization preparation, 3D UTE with a TE of 50 μs /1.5T and 3T Philips scanner	Knee and ankle joints from healthy volunteers	Dual-echo subtraction performed better in terms of scan efficiency and off-resonance behavior for short T2 imaging than the magnetization preparation method.	55
Long T2 suppression using adiabatic IR preparation, 2D UTE with a TE of 80 μs /1.5T GE scanner	Tibia and ankle joints from healthy volunteers	Adiabatic IR preparation method was insensitive to the B1 inhomogeneity.	56
DIR-UTE, 2D UTE with a TE of 8 μs /3T GE scanner	Human patellar and lumbar samples, tibia and ankle joints from healthy volunteers	DIR-UTE sequence was able to highlight short T2 tissues with both long T2 water and fat signals well-suppressed.	53
Dual-echo subtraction and DIR preparation, 2D UTE with a TE of 8 μs /3T GE scanner	Human patellar samples	High signal intensity in OCJ region originated from the calcified cartilage and the deepest layer of the uncalcified cartilage.	14
High resolution 2D UTE with a TE of 30 μs/3T GE scanner	Knee joints from healthy volunteers and patients with knee pain	Healthy controls had a bright line on the OCJ more frequently and with higher signal intensity than in patients with knee pain.	62
T1 weighting and FS preparation, 3D UTE with a TE of 32 μs/3T GE scanner	Patellar sample, knee joints from healthy volunteers and patients with OA	Both long T2 water and fat signals were well-suppressed in T1-weighted FS UTE sequence. Bright OCJ signal lines were seen in normal joints, but absent in abnormal cartilage regions.	57
IR and FS preparation, 3D UTE with a TE of 32 μs/3T GE scanner	Human patellar sample and cadaveric knee joints, knee joints from healthy volunteers and patients with OA	Both long T2 water and fat signals were well-suppressed in IR-FS-UTE sequence. Bright OCJ signal lines were seen in normal joints, but absent in abnormal cartilage regions.	58
DIR-UTE, 3D UTE with a TE of 32 μs /3T GE scanner	Knee joints from healthy volunteers and patients with OA	Both long T2 water and fat signals were well-suppressed in IR-FS-UTE sequence. Bright OCJ signal lines were seen in normal joints, but absent in abnormal cartilage regions.	59
High resolution 3D Cones with a TE of 30 μs/(field strength not provided)	Ovine knee joints	UTE sequence was able to detect the OCJ signal and the associated iron-labeled stem cells with excellent anatomical detail.	63
IR and FS preparation, 3D ZTE with a TE of 12 μs/3T GE scanner	Human cadaveric knee joints, knee joints from healthy volunteers and patients with OA	Both long T2 water and fat signals were well-suppressed in IR-FS-ZTE sequence. Bright OCJ signal lines were seen in normal joints, but absent in abnormal cartilage regions.	74
High resolution 3D SWIFT/9.4T Varian scanner	Osteochondral samples from horse intercarpal and contralateral joints	High-resolution SWIFT imaging was able to assess spontaneous osteochondral repair in an equine model and reveal a large degree of bone detail.	75
Water or fat suppression, high resolution 3D SWIFT/9.4T Varian scanner	Osteochondral samples from human cadaveric knee joints	The bright OCJ signals seen in SWIFT images resided within the noncalcified cartilage region.	77

Author Manuscript Author Manuscript Author Manuscript Author Manuscript

Table 2.

Summary of the UTE techniques for quantitative OCJ imaging

Technique/scanner	Subjects	Main findings	Ref.
2D DIR-UTE for T1, T2*, and T1rho measurements/3T GE scanner	Human patellar samples	T1 ranged from 256 to 389 ms, T2* ranged from 1.0 to 3.3 ms, and T1rho ranged from 2.2 to 4.6 ms.	39
3D UTE T2* measurement/3T GE scanner	Knee joints from healthy volunteers and patients with ACLR	Significant T2* changes were found in deep cartilage region between controls and patients.	64
3D UTE T2* measurement/3T GE scanner	Knee joints from healthy volunteers and patients with ACLR	T2* of deep cartilage was associated with knee mechanical alignment and KAM during walking.	65
3D UTE T2* measurement/3T GE scanner	Knee joints from healthy volunteers and patients with ACLR	Deep cartilage T2* values in the patellofemoral joint showed significant correlation with a worse KOOS sport/rec.	69
2D UTE T2* measurement/7T Bruker scanner	Cartilage-bone rectangular samples extracted from canine humeral head	UTE was capable of reliably measuring T2* of the deep radial and calcified zones of cartilage. The magic angle phenomenon had little effect on UTE MR imaging, especially using bi-exponential methods for model fitting.	12
2D UTE bi-component T2* measurement/3T GE scanner	Human patellar samples	The long T2* values tended to increase from subchondral bone to superficial cartilage, but short T2* remained stable. The short T2* values were also much less insensitive to the magic angle effect than long T2* values.	70
3D UTE T1, T1rho, MMF, and T2* measurements/3T GE scanner	Human cadaveric knee joints	T1, T1rho, and T2* increased from deep to superficial cartilage, while MMF decreased from the OCJ to superficial cartilage. Significant correlations were found between T1, T1rho, MMF, and T2 and the cartilage degeneration MOAKS scores.	71